

## PLANT SCIENCES

# The wound-activated ERF15 transcription factor drives *Marchantia polymorpha* regeneration by activating an oxylipin biosynthesis feedback loop

Yuanke Liang<sup>1,2</sup>, Jefri Heyman<sup>1,2</sup>, Yanli Xiang<sup>1,2</sup>, Wiske Vandendriessche<sup>1,2</sup>, Balkan Canher<sup>1,2</sup>, Geert Goeminne<sup>1,3</sup>, Lieven De Veylder<sup>1,2\*</sup>

The regenerative potential in response to wounding varies widely among species. Within the plant lineage, the liverwort *Marchantia polymorpha* displays an extraordinary regeneration capacity. However, its molecular pathways controlling the initial regeneration response are unknown. Here, we demonstrate that the MpERF15 transcription factor gene is instantly activated after wounding and is essential for gemmaling regeneration following tissue incision. MpERF15 operates both upstream and downstream of the MpCOI1 oxylipin receptor by controlling the expression of oxylipin biosynthesis genes. The resulting rise in the oxylipin dinor-12-oxo-phytodienoic acid (dn-OPDA) levels results in an increase in gemma cell number and apical notch organogenesis, generating highly disorganized and compact thalli. Our data pinpoint MpERF15 as a key factor activating an oxylipin biosynthesis amplification loop after wounding, which eventually results in reactivation of cell division and regeneration. We suggest that the genetic networks controlling oxylipin biosynthesis in response to wounding might have been reshuffled over evolution.

## INTRODUCTION

Being sessile, plants may have evolved many different strategies to restore wounded cells and tissues (1, 2). Frequently, wounding activates transcriptional cascades that contribute to the reprogramming of cell fate to replace damaged cells by reactivation of cell division or to initiate new developmental programs (3). However, even among plants, a huge variation in regeneration potential can be observed. Some species are highly regeneration competent, such as the dicot model plant *Arabidopsis thaliana*, being exemplified by its ability to form de novo roots on detached organs (3, 4). Differently, the regeneration efficiency of, e.g., woody plants is highly variable, depending on genotype and species. Certain tree species, such as specific poplar genotypes, can be easily cloned and propagated by stem cuttings that activate the formation of adventitious roots at the cut site (5). However, many elite trees are less amenable to routine propagation by cuttings (6, 7). In agricultural species, the capacity to regenerate is even worse, as most cereals, including many important food crops such as rice and maize, tend to be recalcitrant to tissue replenishment upon wounding and regenerate poorly from somatic organs (3).

Among the plant lineage, bryophytes, including liverworts, mosses, and hornworts, have relatively simple body structures and are acknowledged for their extraordinary regeneration efficiency, because fully differentiated tissue cells can be reprogrammed to stem cells within 2 days after injury (8, 9). Among the liverworts, *Marchantia polymorpha* represents an emerging plant model system with a long history of regeneration research (10, 11), due to its short life cycle (3 to 4 weeks from spore to mature thallus), haploidy, and small genome size (approximately 218.7 Mb) (12, 13). The mature gametophytic plant body (thallus or thalli) of *M. polymorpha* can reproduce asexually by producing multicellular gemmae in gemma cups

(14). The gemmae are discoid in shape and connected to the gemma cup by a single stalk cell. Two meristematic notches (called apical notches) are placed at both ends of the axis perpendicular to the stalk axis (15). *M. polymorpha* can reacquire stem cells from virtually any cell in mature organs upon injury (16). All cell types in the gametophyte can give rise to whole plant bodies. However, the exact mechanism behind this extraordinary regeneration capacity has not been thoroughly examined.

Wounding modulates endogenous hormonal responses by triggering hormone biosynthesis and/or targeted hormone transport (3, 17). Typically, the inflicted damage activates signaling pathways that eventually results in the reacquisition of stem cell activity at the site of wounding, resulting in the de novo formation of meristems. In flowering plants, regeneration depends on the phytohormone auxin, triggered either through neobiosynthesis or by accumulation resulting from the removal of the basal auxin drain (18–20). The lipid-derived phytohormone jasmonic acid (JA) is considered as another important plant hormone in response to wounding because its accumulation can be detected within seconds after injury (21, 22). JA, as a member of the oxylipin phytohormone family, plays essential roles in plant growth, development, and stress responses by activating a genome-wide reprogramming of gene expression (22). In addition, JA, methyl-JA (MeJA), and other metabolic precursors of jasmonoyl-isoleucine (JA-Ile) are potent elicitors of specialized metabolites and proteins that deter plant enemies (22). In tracheophytes, JA is converted to (+)-7-iso-JA-Ile and perceived by the F-box protein CORONATINE INSENSITIVE1 (COI1), resulting in the ubiquitination and degradation of the JASMONATE-ZIM DOMAIN (JAZ) transcriptional repressors (23, 24), leading to the release of the basic helix-loop-helix transcription factor (TF) MYC2 (25). MYC2 and its homologs bind directly to the promoters of JA-responsive genes to promote their transcription (26).

Genome analysis revealed that the JA signaling pathway first appeared more than 450 million years ago in the common ancestor of extant land plants (12). Although nonvascular plants do not synthesize

Copyright © 2022  
The Authors, some  
rights reserved;  
exclusive licensee  
American Association  
for the Advancement  
of Science. No claim to  
original U.S. Government  
Works. Distributed  
under a Creative  
Commons Attribution  
NonCommercial  
License 4.0 (CC BY-NC).

<sup>1</sup>Department of Plant Biotechnology and Bioinformatics, Ghent University, Ghent B-9052, Belgium. <sup>2</sup>VIB Center for Plant Systems Biology, Ghent B-9052, Belgium. <sup>3</sup>VIB Metabolomics Core, Ghent, Belgium.

\*Corresponding author. Email: lieven.deveylder@psb.vib-ugent.be

JA-Ile, similar to other bryophytes, *M. polymorpha* synthesizes the JA-precursor 12-oxo-phytodienoic acid (OPDA) and its two-carbons-shorter homolog dinor-12-oxo-phytodienoic acid (dn-OPDA), which are recognized by COI1 to activate downstream signaling (12, 27–29). OPDA and dn-OPDA accumulate instantly after wounding and regulate various physiological and developmental processes such as growth, senescence, and stress adaption (27, 30). Biochemically, OPDA and dn-OPDA are synthesized from the fatty acids  $\alpha$ -linolenic acid and hexadecatrienoic acid, respectively, derived from chloroplast membrane lipids. Oxygenation by 13-lipoxygenase (LOX) and dehydration-cyclization by allene oxide synthase (AOS) and allene oxide cyclase (AOC) convert  $\alpha$ -linolenic acid to OPDA and hexadecatrienoic acid to dn-OPDA (31).

Next to hormonal input, the regeneration process depends on a complex network of genetic and epigenetic changes (32). In *Arabidopsis*, the TF ETHYLENE RESPONSE FACTOR 109 (ERF109), a direct target of the JA signaling pathway, was found to serve as an important cross-talk node between JA and auxin signaling. Upon excision of *Arabidopsis* leaves, wounding triggers the immediate accumulation of JA, which activates *ERF109* expression in a COI1- and MYC2-dependent manner, ultimately resulting in the generation of de novo roots from the cut site (17, 19). Subsequently, ERF109 promotes auxin production by activating the tryptophan biosynthesis *ANTHRANILATE SYNTHASE*  $\alpha 1$  (*ASA1*) and *YUCCA 2* (*YUC2*) genes (18–20). ERF109 also stimulates expression of its homologous gene *ERF115* to promote regeneration (17). Eventually, to prevent hypersensitivity to wounding, JAZ repressors physically bind to ERF109 to inhibit its activity to again attenuate the JA-dependent regeneration cascade (19).

Here, we reveal that MpERF15 (Mp7g09350) encodes the functional homolog of *Arabidopsis* *ERF109*, representing a key factor controlling *M. polymorpha* regeneration following tissue incision. Similarly to *Arabidopsis* *ERF109*, its expression was found to depend on COI1 activity, but differently, MpERF15 contributes to OPDA (or dn-OPDA) biosynthesis. Overall, our data pinpoint MpERF15 as a key factor activating an OPDA/dn-OPDA biosynthesis amplification loop that eventually results in cell division reactivation and regeneration.

## RESULTS

### MpERF15 and ERF109 share an evolutionarily conserved wound response

In *Arabidopsis*, members of the subfamily class X of ERF TFs play an important role in wound-induced regeneration, of which several are rapidly induced upon injury (2, 33). On the basis of the presence of the conserved DNA-binding AP2-encoding sequence, 30 ERF genes were found in the *M. polymorpha* genome (MpERF), compared to 147 genes in *Arabidopsis* (AtERF) (2, 12). To reveal the MpERFs involved in the early signaling events after wounding, we carried out an RNA-sequencing (RNA-seq) experiment using 14-day-old wild-type [WT; Takaragaike-1 (Tak-1)] thalli harvested 1 hour following extensive tissue incision, compared to unwounded thalli. Eight MpERF genes were found to be up-regulated more than 1.5-fold after wounding (Fig. 1A). Among these, MpERF15 was strongly activated. The wound responsiveness of MpERF15 was confirmed in 10-day-old gemmalings through quantitative reverse transcription polymerase chain reaction (RT-qPCR), demonstrating MpERF15 transcripts to be more than tenfold induced within 15 min after

wounding and peaking at 1 hour, followed by a strong decline, but still being detectable at 24 hours after wounding (Fig. 1B).

Phylogenetic analysis of MpERF and AtERF subfamily class X members showed that MpERF15 is the closest relative of ERF109 (Fig. 1C). To determine whether MpERF15 and *ERF109* might represent functional orthologs, the MpERF15 ORF was cloned under the control of the *Arabidopsis* 3.1-kb *ERF109* promoter (*ERF109pro:MpERF15*) and introduced into the *erf109* (SALK\_150614) mutant by transformation for complementation analysis. A similar construct driving the *ERF109* gene was used as positive control (*ERF109pro:ERF109*). Because *Arabidopsis* *erf109* mutants display reduced adventitious root formation from leaf explants (19), we performed a de novo root regeneration experiment using detached leaf explants from 12-day-old WT (Col-0), *erf109* mutant, and two independent transgenic lines of *ERF109pro:MpERF15<sup>erf109</sup>* (#1 and #2) and *ERF109pro:ERF109<sup>erf109</sup>* (#1 and #2). After 8 days, around 75% of WT leaves regenerated adventitious roots from the petiole cut, whereas a clear reduction in regeneration (less than 40%) in the *erf109* mutant could be observed, in agreement with previous observations (19). Notably, both *ERF109pro:MpERF15<sup>erf109</sup>* and *ERF109pro:ERF109<sup>erf109</sup>* restored the leaf explant adventitious rooting phenotype (Fig. 1D). Independently, we evaluated the ability to regenerate a de novo root tip 72 hours after removal of the 200- $\mu$ m distal root tip from 7-day-old seedlings. The de novo root meristem formation appeared to be dependent on *ERF109*, because less than 40% of *erf109* roots were able to regenerate a novel stem cell niche, compared to approximately 60% for *Arabidopsis* WT roots (Fig. 1E), in agreement with previous observations that the *erf109* mutant exhibits impaired capacity of root regeneration (17). *erf109* mutant plants holding the *ERF109pro:MpERF15* or *ERF109pro:ERF109* complementation constructs displayed a rescue of this root tip regeneration defect.

Before, the *Arabidopsis* ERF109 protein was demonstrated to bind the JAZ5/8/9 proteins (19). *M. polymorpha* contains one single JAZ protein (MpJAZ), being phylogenetically the most closely related to the subgroup V in *Arabidopsis* (JAZ3/4/9) (34). Using the yeast two-hybrid assay, we observed an interaction between MpERF15 and AtJAZ3, AtJAZ4, AtJAZ9, and MpJAZ (Fig. 1F). *Arabidopsis* ERF109 also interacted with MpJAZ. Combined, these results strongly indicate that *M. polymorpha* MpERF15 and *Arabidopsis* ERF109 are functionally equivalent proteins.

### Regeneration defect of Mper15<sup>ko</sup>

To analyze the role of MpERF15 during *M. polymorpha* regeneration, we generated several independent frameshift mutant lines *Mper15<sup>ko</sup>* (#9, #10, and #13) in the Tak-1 background using CRISPR-Cas9 (fig. S1A). Under normal vegetative growth conditions, these *Mper15<sup>ko</sup>* mutants did not show a notable growth phenotype, displaying normal gemma, thalli, and gemma cup development (fig. S1, B and C). Next, the mutants were tested for their ability to regenerate. WT Tak-1 and *Mper15<sup>ko</sup>* gemmae were isolated from the gemma cups and cultured in liquid medium for 2 days. Subsequently, explant fragments without meristematic tissues were generated by surgical removal of the apical notches from the gemmalings (Fig. 2A) and allowed to grow on agar under continuous white light. Three days following apical notch resectioning, tissue growth was observed near the wound edges of Tak-1, being more pronounced at 4 days after excision, whereas for the *Mper15<sup>ko</sup>* thalli, a clear delayed regeneration of tissue at the wound edges could be observed

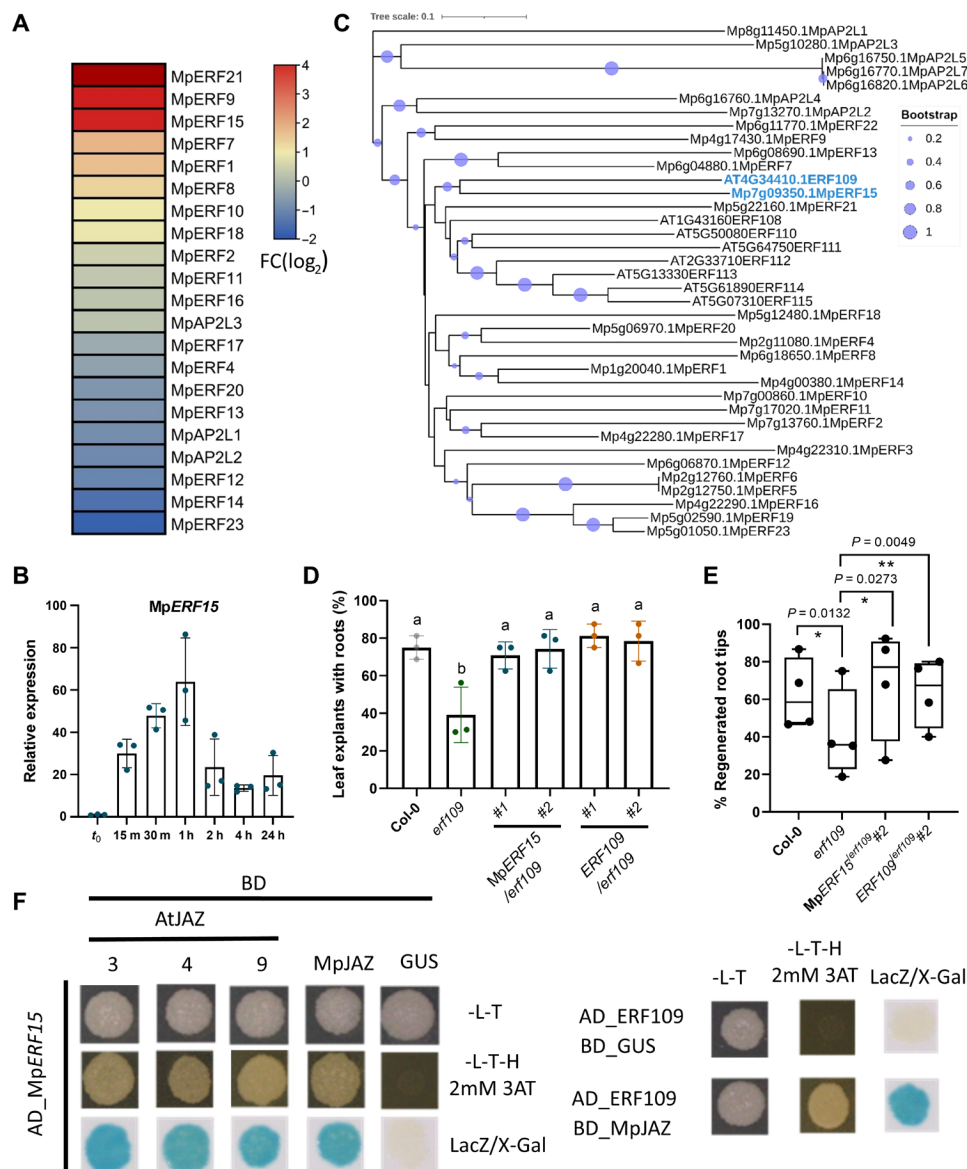


**Fig. 1. *Marchantia* MpERF15 shows functional conservation with *Arabidopsis* ERF109.** (A) Heatmap of MpERF expression after wounding. Fold changes (FCs) represent  $\log_2$  values of the number of transcripts per kilobase of exon model per million mapped reads of 14-day-old Tak-1 thallus 1 hour after wounding compared to unwounded. (B) RT-qPCR analysis of MpERF15 transcripts in 10-day-old Tak-1 gemmings following tissue incision ( $n = 3$ , six plants per replicate). (C) Phylogenetic analysis of *Arabidopsis* subfamily X and *Marchantia* ERFs. (D) Percentages of Col-0, *erf109*, *ERF109pro:MpERF15<sup>erf109</sup>*, and *ERF109pro:ERF109<sup>erf109</sup>* that regenerated adventitious roots on leaf explants following transfer for 8 days on B5 medium ( $n = 3$ , >16 plants per replicate). Letters indicate significant differences [one-way analysis of variance (ANOVA)/post hoc Tukey honestly significant difference (HSD) test  $P < 0.05$ ] between genotypes. (E) Root tip excision recovery of 7-day-old Col-0, *erf109*, *ERF109pro:MpERF15<sup>erf109</sup>* #2, and *ERF109pro:ERF109<sup>erf109</sup>* #2 at 72 hours after removing the 200- $\mu$ m distal root tip ( $n = 4$ , >16 plants per replicate). Significance was calculated using Fisher's exact test. (F) Yeast two-hybrid assays showing AtJAZ3, AtJAZ4, AtJAZ9, and MpJAZ interaction with MpERF15, and MpJAZ with AtERF109. Yeasts were grown onto SD/-Trp/-Leu (-L-T) and SD/-His/-Trp/-Leu (-L-T-H) with 2 mM 3AT media. Blue LacZ/X-Gal test indicates a positive interaction. Negative controls: GUS BD + MpERF15-AD and GUS-BD + AtERF109-AD. AD, GAL4 activation domain; BD, GAL4 binding domain.

(Fig. 2B). Measurement of the size of the regenerated tissue showed that all three *Mperif15<sup>ko</sup>* (#9, #10, and #13) mutants displayed a significant regeneration defect compared to Tak-1 (Fig. 2C). Likewise, 10-day-old *Mperif15<sup>ko</sup>* gemmaling basal explants exhibited a slow regeneration response that was maintained over a period of at least 8 days (fig. S2, A and B). These data illustrate that MpERF15 plays an important role in gemmaling regeneration following apical notch removal.

Given that the *ASA1* gene was defined as a wound-inducible target of *ERF109* in *Arabidopsis* (19), we tested whether MpASA1 (Mp2g26760) expression was affected by wounding in the *Mperif15<sup>ko</sup>* lines. Fourteen-day-old Tak-1 and *Mperif15<sup>ko</sup>* (#9, #10, and #13) mutant thalli were extensively incised and sampled for RT-qPCR analysis at 1, 2, and 4 hours after wounding. *Mperif15<sup>ko</sup>* (#9, #10, and #13) mutants displayed a significant reduction in MpASA1 expression at 4 hours after wounding compared to the WT (Fig. 2D). These data again

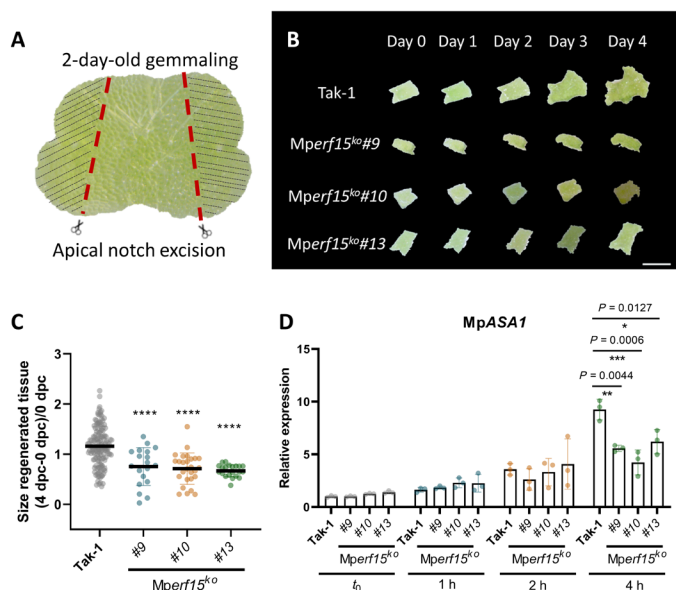


**Fig. 2. MpERF15 is essential for gemmaling regeneration after wounding.** (A) Two-day-old gemmalings were excised along the red dashed lines to prepare pieces without apical notches (shadowed). (B) Time-lapse registration over 4 days of the regeneration of 2-day-old Tak-1 and *Mper15*<sup>ko</sup> gemmalings excised as shown in (A) under continuous white light. Scale bar, 1 mm. (C) Quantification of Tak-1 and *Mper15*<sup>ko</sup> regenerated apical notches 4 days post-cut (dpc). Regeneration was calculated by plotting the ratio of 4 dpc minus 0 dpc to 0 dpc explant sizes. Data represent means  $\pm$  SD. Dots represent individual data points ( $n > 20$ ). Statistical differences of each *Mper15*<sup>ko</sup> mutant compared to Tak-1 were evaluated with Student's *t* test; \*\*\*\* $P < 0.0001$ . (D) RT-qPCR analysis of *MpASA1* in Tak-1 and *Mper15*<sup>ko</sup> mutants from  $t_0$  to 4 hours after wounding. Data represent the mean relative expression compared to the unwounded Tak-1  $\pm$  SD ( $n = 3$ , six plants per replicate); the asterisks indicate significant differences (one-way ANOVA/post hoc Tukey HSD test) of each *Mper15*<sup>ko</sup> mutant compared to Tak-1.

suggested that *MpERF15* is functionally related to *ERF109* and plays an important role in the wound response.

### MpERF15 affects expression of OPDA/dn-OPDA biosynthesis genes

To map the genome-wide spectrum of *MpERF15*-responsive genes, we performed an RNA-seq study using 14-day-old WT Tak-1 and mutant *Mper15*<sup>ko</sup> thalli, either unwounded or harvested 1 hour after wounding. A total of 856 differentially expressed genes were found between Tak-1 and *Mper15*<sup>ko</sup> in the absence of wounding (187 being up-regulated and 669 down-regulated) (data S1). Gene Ontology (GO) analysis of the down-regulated genes in *Mper15*<sup>ko</sup> highlighted the enrichment for categories related to diverse metabolic and catabolic processes, including those related to JA and oxylipin biosynthesis (fig. S3A and data S2). Confirming the involvement of *MpERF15* in JA-related pathways, we found a significant overlap between genes down-regulated in *Mper15*<sup>ko</sup> and the previously reported *MpCOI1*-dependent cluster or genes up-regulated in the *Mpjaz-1* mutant (Fig. 3A) (27, 34). These data suggested that *MpERF15* and *MpCOI1* may operate in the same pathway. Accordingly, *MpERF15* expression was strongly reduced in 14-day-old *Mpcoi1-2* thalli, both with and without wounding (Fig. 3B). Reversely, *MpCOI1* expression did not depend on *MpERF15*, neither under control ( $t_0$ ) or wounding conditions (2 or 4 hours; Fig. 3C). In both WT Tak-1

and *Mpcoi1-2* thalli, *MpERF15* was ninefold transcriptionally induced after wounding (Fig. 3B). These results indicate that *MpERF15* is a downstream target of *MpCOI1*, but its wound responsiveness is *MpCOI1* independent.

To map the role of *MpERF15* in the wound response pathway, we selected within our generated RNA-seq dataset genes that are wound inducible in an *MpERF15*-dependent manner, yielding a total of 172 genes (Fig. 3D and data S3). GO term analysis of this subcategory of genes highlighted responses to stress and regulation of metabolic processes (fig. S3B and data S4). Four *Dirigent-like protein* genes belong to the wound-inducible and *MpERF15*-dependent gene cluster (*MpDIR17*, *MpDIR38*, *MpDIR42*, and *MpDIR43*). Among these, *MpDIR38* (Mp5g16520) has been identified before as a wound-inducible marker (27, 29, 35) and was confirmed by RT-qPCR to be *MpERF15* dependent (fig. S3C). Among the gene list, we also identified the OPDA and dn-OPDA biosynthesis genes *MpAOS2* (Mp5g16260) and *MpAOC* (Mp7g06220). Accordingly, RT-qPCR data confirmed that the transcript levels of *MpAOS2* and *MpAOC* were not significantly different between Tak-1, *Mper15*<sup>ko</sup>, and *Mpcoi1-2* in the absence of wounding, but the increase in transcript levels following tissue damage was significantly lower in *Mper15*<sup>ko</sup> for *MpAOS2* (Fig. 3E) or in both *Mper15*<sup>ko</sup> and *Mpcoi1-2* for *MpAOC* (Fig. 3F). These data suggested that although *MpERF15* acts as a downstream target of *MpCOI1*, it may regulate OPDA biosynthesis, thus representing a potential feedback loop.

### OPDA/dn-OPDA biosynthesis is controlled by MpERF15 and essential for regeneration

Because of the observed GO enrichment for different metabolic processes being controlled in an *MpERF15*- and wound-inducible manner, we performed an untargeted metabolomics experiment comparing WT Tak-1 versus *Mper15*<sup>ko</sup> mutants before and 1 hour after wounding. In total, 5159 and 5369 compound ions were detected by electrospray ionization (ESI) operating in a negative (–) or positive (+) mode, respectively (data S5). The distance dendrogram showed that Tak-1 and *Mper15*<sup>ko</sup> mutants were mixed over both clusters before wounding, whereas they separated into two clusters after damage (fig. S4, A and B), suggesting that the metabolome of undamaged Tak-1 and *Mper15*<sup>ko</sup> was much alike, whereas their post-damage metabolome differed. In total, we detected 88 and 48 compound ions in ESI– and ESI+ modes, respectively, which were highly induced after 1 hour of wounding but dependent on *MpERF15* (fig. S4, C and D, and data S6). On the basis of database searches (NIST20), we detected OPDA/dn-OPDA and their precursors in trace amounts in both Tak-1 and *Mper15*<sup>ko</sup> mutants before wounding, whereas the normalized abundance of these compounds increased substantially in both Tak-1 and the *Mper15*<sup>ko</sup> mutants 1 hour after wounding (Fig. 3, G and H, and data S6). However, the abundance was at least more than two- to threefold lower in *Mper15*<sup>ko</sup> mutants compared to WT Tak-1. OPDA and dn-OPDA were further confirmed through comparison with an authentic standard (fig. S5, A and B).

Because *MpAOC* performs a key step in OPDA/dn-OPDA biosynthesis (fig. S6A) (30), whose corresponding gene is transcriptionally controlled by *MpERF15*, we generated *Mpaoc*<sup>ko</sup> mutants by CRISPR-Cas9 technology. Two independent mutants, *Mpaoc*<sup>ko</sup> #1 and #4, were confirmed by sequencing (fig. S6B). Notably, similar to *Mper15*<sup>ko</sup> thalli, both *Mpcoi1-2* and *Mpaoc*<sup>ko</sup> exhibited a slow regeneration response following 2- and 10-day-old gemmaling incision (Fig. 3I and fig. S2,

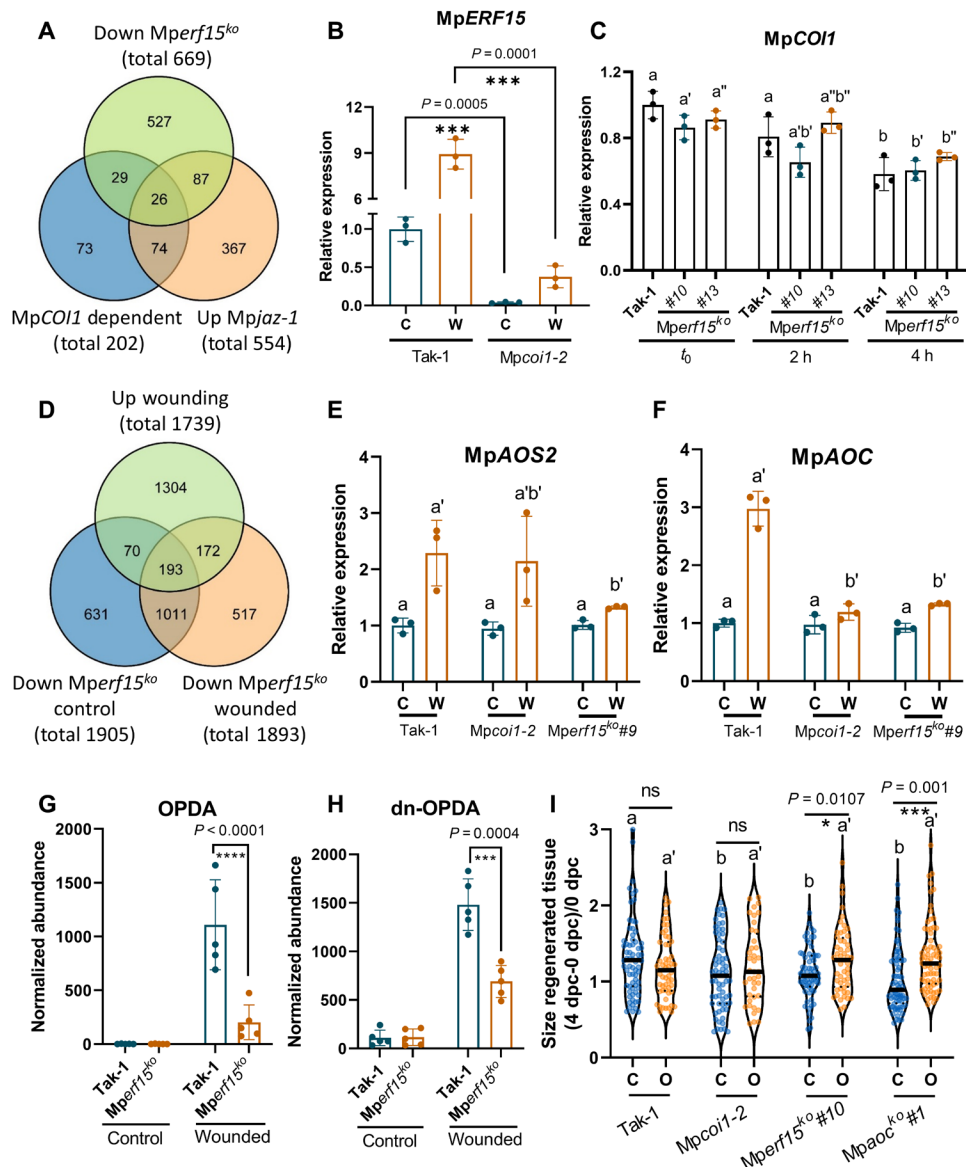


**Fig. 3. MpERF15 drives expression of oxylipin biosynthesis genes.** (A) Overlap of genes down-regulated in *Mper15<sup>ko</sup>* before wounding, *MpCOI1*-dependent genes, and genes up-regulated in *Mpjz-1*. (B) RT-qPCR analysis of *MpERF15* transcript levels in 14-day-old Tak-1 and *Mpcoi1-2* thallus in unwounded control conditions (C) and 1 hour after wounding (W). (C) RT-qPCR analysis of *MpCOI1* transcript levels in Tak-1 and *Mper15<sup>ko</sup>* after wounding from  $t_0$  to 4 hours. (D) Overlap of genes up-regulated in Tak-1 1 hour after wounding and down-regulated in *Mper15<sup>ko</sup>* in control conditions or 1 hour after wounding. (E and F) RT-qPCR analysis of *MpAOS2* (E) and *MpAOC* (F) in 14-day-old Tak-1, *Mpcoi1-2*, and *Mper15<sup>ko</sup>#9* thallus in control conditions and 1 hour after wounding. (G and H) Normalized abundance of OPDA (G) and dn-OPDA (H) compounds in Tak-1 and *Mper15<sup>ko</sup>* in control conditions and 1 hour after wounding in ESI<sup>−</sup> mode. (I) Effect of apical notch excision on the regeneration of 2-day-old Tak-1, *Mpcoi1-2*, and *Mpaoc<sup>ko</sup>* control (C) gemmings compared with those treated for 2 hours with 10 nM OPDA (O),  $n > 15$ . (B and G to I) Asterisks indicate significant differences by Student's *t* test. ns, nonsignificant. (C, E, F, and I) The different letters indicate significant differences (two-way ANOVA/post hoc Tukey HSD test,  $P < 0.05$ ) between each genotype.

A and B). A 2-hour treatment with 10 nM OPDA rescued the regeneration defect of *Mpaoc<sup>ko</sup>* and *Mper15<sup>ko</sup>*, but not of the *Mpcoi1-2* mutant (Fig. 3I). Together, these data confirm that OPDA is essential for regeneration after wounding.

### MpERF15 promotes oxylipin accumulation causing hyperproliferation

To confirm the observed role for MpERF15 in regeneration and OPDA/dn-OPDA biosynthesis, we generated three independent lines

overexpressing MpERF15 from the constitutive promoter *MpEF1 $\alpha$*  (*ELONGATION FACTOR 1 $\alpha$* , Mp3g23400) in WT Tak-1 (named *MpERF15<sup>OE</sup>* #1, #2, and #7) (Fig. 4A). All 14-day-old lines displayed an approximately 20- to 30-fold increase in *MpERF15* expression level compared to WT Tak-1 (fig. S7A). At a mature developmental stage, *MpERF15<sup>OE</sup>* thalli exhibited a highly disorganized and compact appearance, and its growth rate was significantly slower than that of Tak-1 (Fig. 4, A and B). Ectopic overexpression of *Arabidopsis ERF109* in *M. polymorpha* using the constitutive promoter *CaMV*

35S (named *ERF109<sup>OE</sup>* #1 and #2) exhibited a similar smaller and more compact appearance, although less pronounced (Fig. 4A and fig. S7B), which might be due to the difference in promoters used. To map the origin of this growth phenotype, a cellular analysis was performed. Whereas *Mperfl5<sup>ko</sup>* gemmae did not show any significant

difference in the number and size of epidermal cells, the number of epidermal cells in *MpERF15<sup>OE</sup>* gemmae was significantly higher than in WT Tak-1, whereas there was no significant difference in gemma size, indicative for a reduction in cell size (Fig. 4, C to E). In addition, we found the number of apical notches in individual *MpERF15<sup>OE</sup>* gemmae to vary from three to nine, whereas WT Tak-1 and *Mperfl5<sup>ko</sup>* gemmae invariably hold only two meristematic notches at both ends of the axis perpendicular to their stalk axis (Fig. 4, F to H, and fig. S1C). Using the *proMpEF1 $\alpha$ :Tdtomato-N7* nuclear localization marker, allowing easy visualization of the apical notches as bright fluorescent foci due to the small size of the apical notch cells, we found the number of concave structures in 8-day-old *MpERF15<sup>OE</sup>* gemmalings to be higher than the two apical notches observed in Tak-1 (Fig. 4I). To investigate whether the ectopic concave structures in *MpERF15<sup>OE</sup>* function as meristems, we introduced the *MpERF15<sup>OE</sup>* expression vector in the apical notch marker line *proMpYUC2:GUS* (36, 37). Overexpression of *MpERF15* resulted in approximately eight blue GUS dots in the 10-day-old thallus, being significantly more than the four blue dots in the Tak-1 background (Fig. 4, J and K). These phenotypes could be reproduced as well using a dexamethasone (DEX)-inducible gene expression system. *proMpEF1 $\alpha$ :MpERF15<sup>GR</sup>* overexpression lines holding the *proMpUBE:mScarlet-LTI6b* plasma membrane localization marker displayed strong morphological changes upon DEX treatment, being identical to those of the constitutively expressing lines, i.e., a dwarfed compact thallus structure (fig. S7, C and D). The *mScarlet* fluorescence confirmed more ectopic concave structures of *proMpEF1 $\alpha$ :MpERF15<sup>GR</sup>* upon DEX treatment (fig. S7C).

To study the dependence of the observed phenotypes on COI1, we overexpressed *MpERF15* in the *Mpcoi1-2* mutant background (*MpERF15<sup>OE</sup>/Mpcoi1-2*; Fig. 5I). To confirm the increase in number of meristematic notches, we visualized cell cycle activity through 5-ethynyl-20-deoxyuridine (EdU) staining (8), which allows labeling of nuclei undergoing DNA replication. All Tak-1 gemmae contained only two EdU-positive concave structures, whereas *MpERF15<sup>OE</sup>* showed more than six EdU-positive concave structures (Fig. 5, A and B). Notably, loss of function of *MpCOI1* rescued the apical notch phenotype, rendering *MpERF15<sup>OE</sup>* lines, showing only two apical notches and EdU-positive concave structures (Fig. 5, C to E). Also, the *MpERF15<sup>OE</sup>*-induced increase in cell number and decrease in cell size were *MpCOI1* dependent, because they were not observed in *MpERF15<sup>OE</sup>/Mpcoi1-2* gemmae (Fig. 5, F to H).

Fitting with a role for *MpERF15* in wound-induced OPDA/dn-OPDA biosynthesis, as suggested by the lack of wound-induced expression of *MpAOS2* and *MpAOC* in the *Mperfl5<sup>ko</sup>* mutants (Fig. 3, E and F), both genes were significantly up-regulated in *MpERF15<sup>OE</sup>*, but not in *MpERF15<sup>OE</sup>/Mpcoi1-2* (Fig. 5, J and K), suggesting that *MpERF15* may promote oxylipin accumulation in an *MpCOI1*-dependent manner. We therefore performed an untargeted metabolomics experiment comparing Tak-1 versus two independent *MpERF15<sup>OE</sup>* lines. As expected from the strong phenotypes (Fig. 4A), principal components analysis (PCA) showed both *MpERF15<sup>OE</sup>* lines to separate from Tak-1 (fig. S8, A and B). ESI- and ESI+ detected 8383 and 11,009 compound ions, respectively, among which 1720 (1085 up-regulated and 635 down-regulated) and 1419 (942 up-regulated and 477 down-regulated) differential compound ions when comparing both *MpERF15<sup>OE</sup>* lines with Tak-1 (fig. S8, C and D, and data S7). Strikingly, we revealed an increase in dn-OPDA in the *MpERF15<sup>OE</sup>* lines compared to Tak-1 (Fig. 6A and fig. S8E), but OPDA was below the

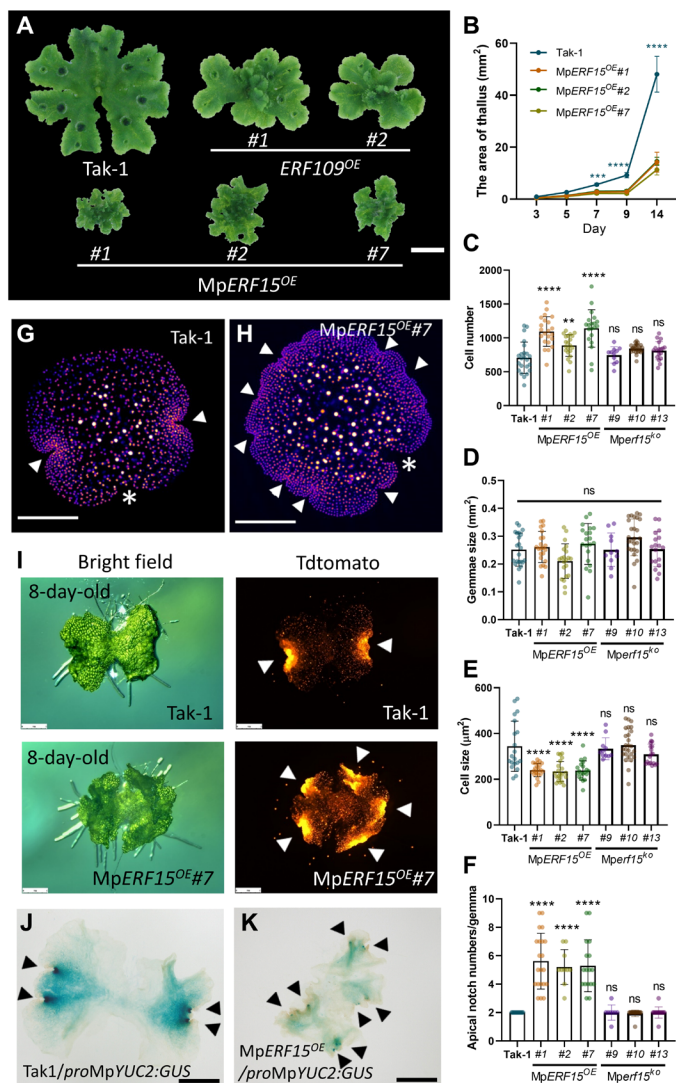


**Fig. 4. *MpERF15* causes an increase in apical notches.** (A) Phenotypic comparisons of 28-day-old Tak-1, *ERF109<sup>OE</sup>*, and *MpERF15<sup>OE</sup>* plants. (Scale bar, 1 cm.) (B) Thallus area of individual Tak-1 and *MpERF15<sup>OE</sup>* lines grown for 3, 5, 7, 9, and 14 days ( $n > 5$ ). Significance was calculated on the basis of two-way ANOVA followed by Tukey's post: \*\*\* $P < 0.001$  and \*\*\*\* $P < 0.0001$ . (C to F) Number of cells in the top epidermal cell layer (C), gemma size (D), average cell size (E), and the number of apical notches per gemma (F) of 0-day-old Tak-1, *MpERF15<sup>OE</sup>*, and *Mperfl5<sup>ko</sup>* gemmae ( $n > 8$ ). Significance was calculated on the basis of one-way ANOVA followed by Tukey's post hoc test compared to Tak-1. \*\* $P < 0.01$  and \*\*\*\* $P < 0.0001$ . (G and H) Confocal imaging of 0-day-old gemmae with *proMpEF1 $\alpha$ :Tdtomato-N7* in a Tak-1 (G) or *MpERF15<sup>OE</sup>* (H) background. Scale bars, 0.1 mm. (I) Bright-field and Tdtomato (red) fluorescence images of 8-day-old gemmalings from Tak-1 and *MpERF15<sup>OE</sup>*. Scale bars, 0.5 mm. (G to I) The white arrowheads indicate the apical notches, and asterisks indicate the stalk cells. (J and K) *proMpYUC2:GUS* staining of 10-day-old thallus in a Tak-1 or *MpERF15<sup>OE</sup>* background. The black arrowheads indicate the blue GUS dots. Scale bars, 1 mm.

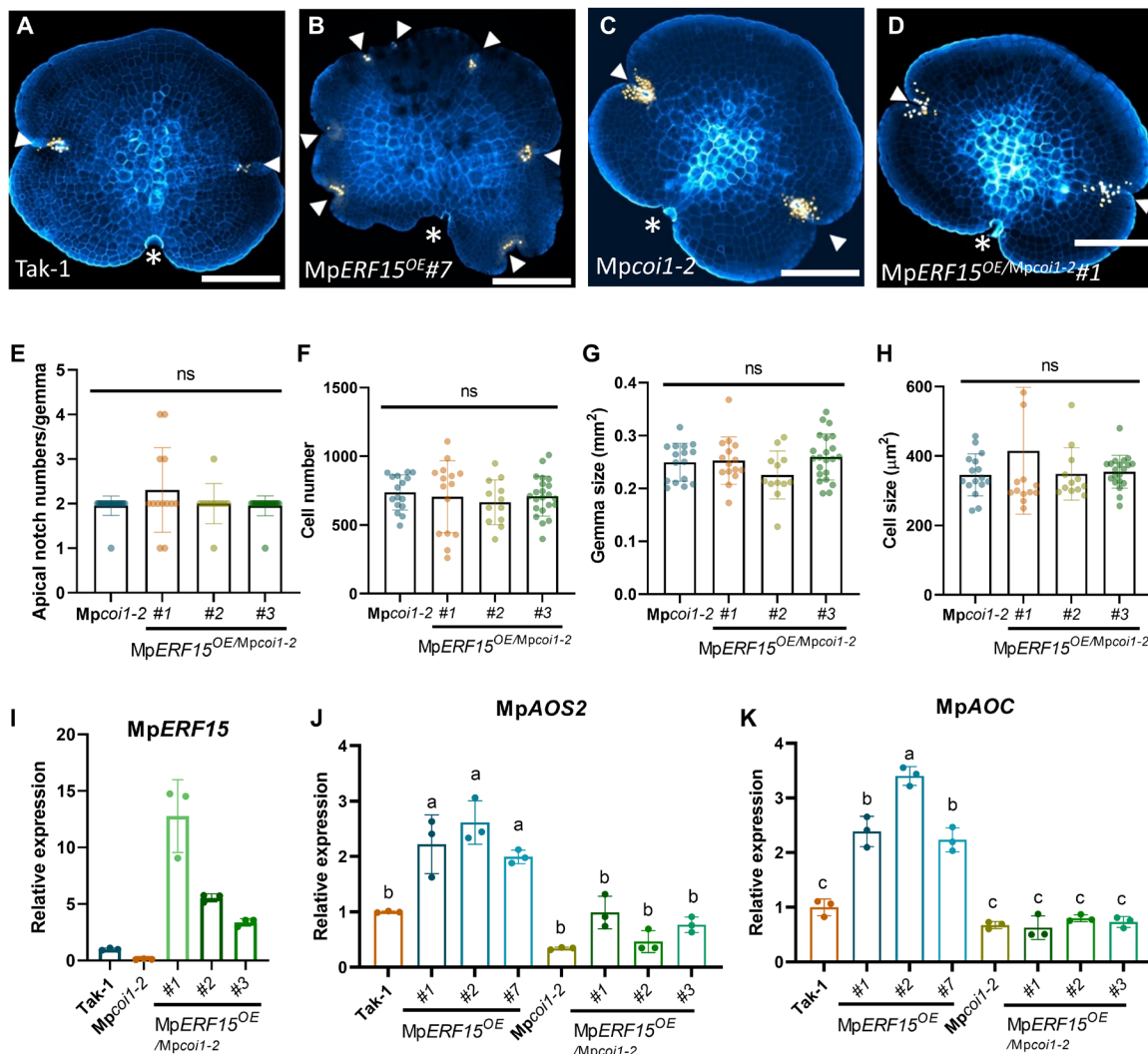


**Fig. 5. MpERF15-induced phenotypes depend on MpCOI1.** (A to D) One-day-old gemmae from Tak-1 (A), MpERF15<sup>OE</sup>#1 (B), Mpcoi1-2 (C), and MpERF15<sup>OE</sup>/Mpcoi1-2#1 (D) labeled by EdU to visualize cell cycle activity and stained with calcofluor white to visualize cell walls. Scale bars, 0.2 mm. The white arrowheads indicate EdU-positive signals, and the asterisks indicate the stalk cells. (E to H) Number of apical notches per gemma (E), number of cells in the top epidermal cell layer (F), gemma size (G), and average cell size (H) of 0-day-old Mpcoi1-2 and MpERF15<sup>OE</sup>/Mpcoi1-2 gemmae ( $n > 12$ ). Significance was calculated on the basis of one-way ANOVA followed by Tukey's post hoc test compared to Mpcoi1-2. (I) RT-qPCR analysis of MpERF15 transcripts in 14-day-old Tak-1, Mpcoi1-2, and independent MpERF15<sup>OE</sup>/Mpcoi1-2 lines. (J and K) RT-qPCR analysis of oxylipin biosynthesis-related genes MpAOS2 (J) and MpAOC (K) in 14-day-old Tak-1, MpERF15<sup>OE</sup>, Mpcoi1-2, and MpERF15<sup>OE</sup>/Mpcoi1-2. The different letters indicate significant differences (one-way ANOVA/post hoc Tukey HSD test,  $P < 0.01$ ) between each genotype.

detection limit and could therefore not be detected in both Tak-1 and MpERF15<sup>OE</sup>. This indicates that MpERF15 enhances biosynthesis of dn-OPDA.

Because of the observed increase in dn-OPDA in the MpERF15<sup>OE</sup> lines, we tested the sensitivity of MpERF15<sup>OE</sup> to OPDA and dn-OPDA. Tak-1, Mpcoi1-2, Mper15<sup>ko</sup>#9, MpERF15<sup>OE</sup>#7, and MpERF15<sup>OE</sup>/Mpcoi1-2#1 gemmae were grown on plates with or without 10 μM OPDA or dn-OPDA. As described before, Tak-1 showed a strong growth reduction in the presence of OPDA/dn-OPDA, whereas Mpcoi1-2 was slightly sensitive to dn-OPDA (Fig. 6, B to D) (27, 38). The MpERF15<sup>OE</sup> thalli appeared to be hypersensitive to OPDA/dn-OPDA, compared to Tak-1 (Fig. 6B), likely because of an already higher intrinsic dn-OPDA level. This growth inhibitory effect was lost in MpERF15<sup>OE</sup>/Mpcoi1-2#1, demonstrating MpCOI1 dependence. In contrast, Mper15<sup>ko</sup>#9 thalli

showed a growth phenotype being in between that of Tak-1 and Mpcoi1-2, thus showing reduced sensitivity (Fig. 6, B to D).

### MpERF15 induces an oxylipin biosynthesis positive feedback loop

Although our data indicated that OPDA biosynthesis is MpERF15 dependent (Fig. 3G), the application of OPDA resulted in an increased expression of MpERF15 (Fig. 7A), suggesting a potential feedback loop in which OPDA stimulates its own biosynthesis. To test this hypothesis, we measured the MpERF15 expression levels in the 7-day-old MpERF15<sup>OE</sup> gemmalings using RT-qPCR primers that recognize only the endogenous MpERF15 transcripts through binding at either 5' untranslated region (5'UTR) and 3'UTR sequences absent in transcripts produced from the MpERF15 overexpression

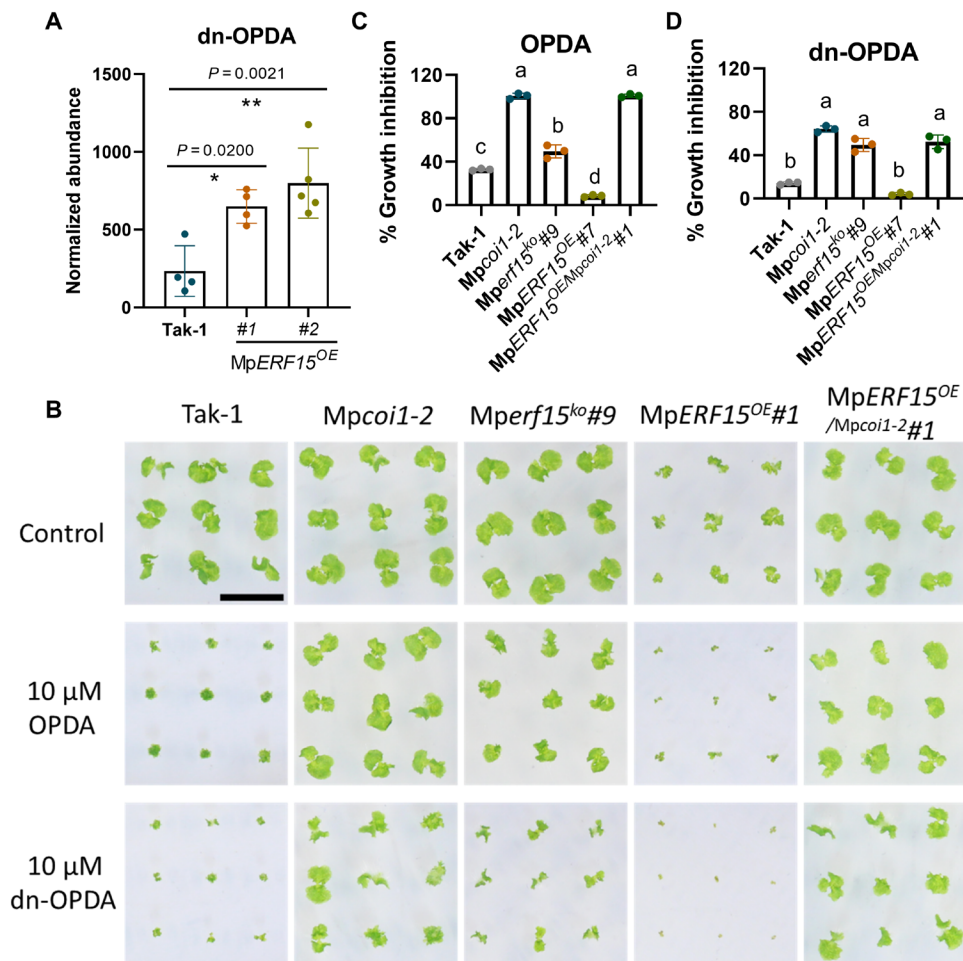


**Fig. 6. MpERF15 induces dn-OPDA biosynthesis.** (A) Normalized abundance of dn-OPDA levels in 14-day-old Tak-1 and MpERF15<sup>OE</sup> in negative (ESI<sup>-</sup>) ionization mode. Data represent means  $\pm$  SD ( $n = 5$ , 12 plants per replicate). Significance was calculated on the basis of one-way ANOVA/post hoc Tukey HSD test of each genotype compared to Tak-1, \* $P < 0.05$  and \*\* $P < 0.01$ . (B) Growth inhibitory effect of 10  $\mu$ M OPDA/dn-OPDA on 10-day-old *Marchantia* gemmalings of WT Tak-1, Mpcoi1-2, Mper15<sup>ko</sup>#9, MpERF15<sup>OE</sup>#7, and MpERF15<sup>OE</sup>/Mpcoi1-2#1. Scale bar, 1 cm. (C and D) Percentage of thalli growth inhibition of WT Tak-1, Mpcoi1-2, Mper15<sup>ko</sup>#9, MpERF15<sup>OE</sup>#7, and MpERF15<sup>OE</sup>/Mpcoi1-2#1 by 10  $\mu$ M OPDA (C) and dn-OPDA (D) compared to growth on control medium. Data represent medians ( $n = 3$ , >5 plants per replicate). The different letters indicate significant differences (one-way ANOVA/post hoc Tukey HSD test,  $P < 0.01$ ) between each genotype.

construct. Using this setup, we found that overexpression of MpERF15 stimulated endogenous MpERF15 transcription, which was dependent on MpCOI1 (Fig. 7, B and C, and fig. S9A), demonstrating that MpCOI1 is an essential part of the positive feedback loop, fitting the observed loss of MpERF15<sup>OE</sup> phenotypes in the Mpcoi1-2 mutant background (Fig. 5, C to H).

### **Arabidopsis ERF109 does not activate a JA biosynthesis feedback loop**

The observed oxylipin biosynthesis feedback loop between COI1 and MpERF15, combined with the functional homology between MpERF15 and ERF109, prompted us to test whether a similar mechanism might hold true in *Arabidopsis*. First, we checked the transcript level of JA biosynthesis-related genes before and 1 hour after wounding in 14-day-old WT Col-0 versus *erf109* mutant seedlings by RT-qPCR. Although all tested genes were up-regulated after wounding, there were no significant differences between Col-0, *erf109*, and *ERF109pro:ERF109<sup>erf109</sup>* complementation lines (Fig. 8A). These

data appeared to indicate that *ERF109* does not play a role in regulating JA biosynthesis. Second, 5-day-old *Arabidopsis* Col-0, *coi1-2*, and *erf109* mutants and the *erf109 ERF109pro:MpERF15<sup>erf109</sup>* complementation line were grown for 7 days on control medium or medium supplemented with 1, 10, or 50  $\mu$ M JA. Except for *coi1-2* that showed a JA-resistant growth phenotype, as described previously (39, 40), no difference in root growth could be observed for the other lines (Fig. 8, B and C). These results indicated that *Arabidopsis ERF109* lost the ability to modulate JA levels during the evolutionary process.

### **MpERF15 operates upstream of MpERF20/LAXR**

Recently, another ERF TF, MpERF20/LAXR (Mp5g06970), has been reported to be wound inducible in the basal part of cut thalli, controlling cellular reprogramming after wounding (11). Its relatively late wound inducibility (6 hours after wounding) suggested that MpERF20/LAXR might operate downstream of MpERF15. We therefore tested the expression levels of MpERF20/LAXR at a late

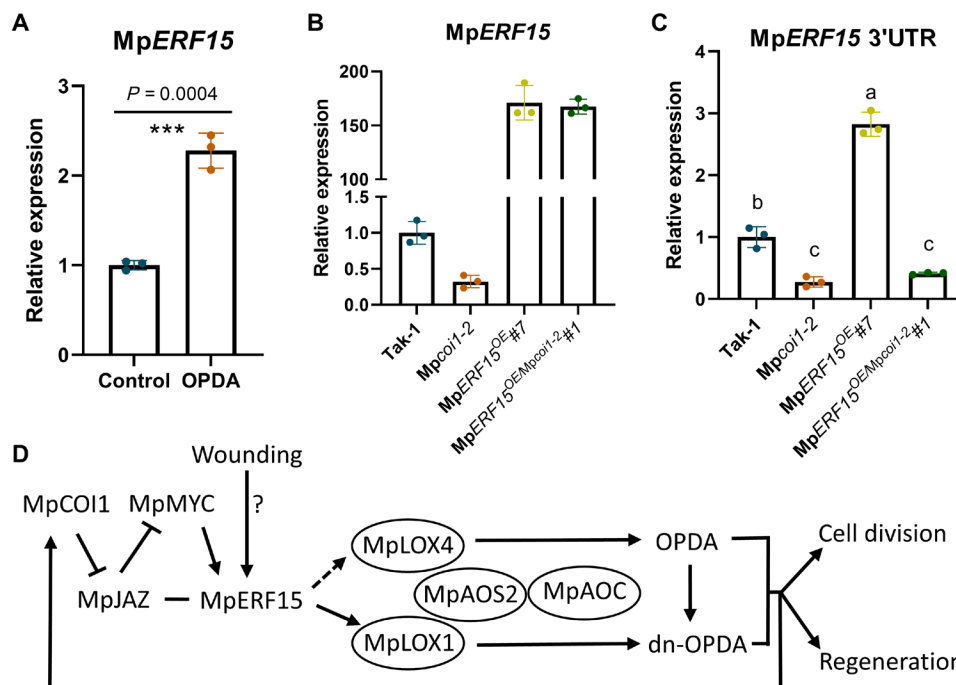


**Fig. 7. MpERF15 is part of an MpCOI1-(dn)-OPDA-dependent feedback loop.** (A) RT-qPCR analysis of *MpERF15* in 14-day-old WT Tak-1 thalli after transfer to control medium (EtOH) or medium supplemented with 10  $\mu$ M OPDA for 2 hours. Data represent the mean relative expression compared to Tak-1  $\pm$  SD ( $n = 3$ , six plants per replicate). Statistical differences were evaluated using Student's *t* test, \*\*\* $P < 0.001$ . (B and C) RT-qPCR analysis of *MpERF15* (B) and *MpERF15* 3'UTR. (C) Transcript levels in 7-day-old Tak-1, *Mpcoi1-2*, *MpERF15<sup>OE</sup>#7*, and *MpERF15<sup>OE</sup>/Mpcoi1-2#1*. Data represent the mean relative expression compared to Tak-1  $\pm$  SD ( $n = 3$ , six plants per replicate). The different letters indicate significant differences (one-way ANOVA/post hoc Tukey HSD test,  $P < 0.01$ ) of each genotype. (D) Schematic diagram of *MpERF15* activating a positive OPDA and dn-OPDA amplification loop that eventually results in reactivation of cell division and regeneration. Arrows represent activation; the dashed arrow points to likely control by another regulator; bar-headed lines represent repression; the line represents interactions between *MpERF15* and *MpJAZ*; the wound-derived *MpERF15*-activating signal is still unknown (indicated by question mark).

stage after wounding and found its wound inducibility to be partially dependent on *MpCOI1*, *MpAOC*, and *MpERF15* (fig. S10A). Reciprocally, *MpERF20/LAXR* transcription was significantly high in *MpERF15<sup>OE</sup>* thalli compared to WT Tak-1 (fig. S10B).

## DISCUSSION

*Arabidopsis* members of the ERF subfamily class X play important roles during regeneration (2, 33). Among these, *ERF109* expression is JA dependent and controls the expression of auxin biosynthesis-related genes, as well as *ERF115* (17–19). *ERF115* itself imposes stem cell fate on the cells immediately adjacent to the wounded cells by increasing their auxin sensitivity, enabling these cells to replace the damaged ones through cell division (41–44). Correspondingly, plants being impaired in *ERF109* or *ERF115* activity display regeneration defects (17, 19, 41, 42, 44). Here, we demonstrate that the extraordinary regenerative potential of *M. polymorpha* relies on the activity of a related ERF protein, suggesting an early evolutionary establishment of ERF subfamily TFs as regeneration-driving components.

*MpERF15* is phylogenetically and functionally most closely related to *Arabidopsis* *ERF109*, with the expression of both genes depending on the COI1 receptor, and both proteins associating with JAZ proteins and controlling *ASA1* expression. Furthermore, like *ERF109*, *MpERF15* is a likely target of the *M. polymorpha* homolog of MYC2 that coordinates JA-mediated transcriptional responses (17), because available microarray data (GSE124159) show that *MpERF15*

expression is suppressed in the *Mpmyc* mutant upon wounding or OPDA treatment (fig. S9B) (29). Accordingly, we demonstrated that *MpERF15* allows to restore the *erf109* regeneration defects in *Arabidopsis*, whereas ectopic expression of *ERF109* in *M. polymorpha* triggers a growth phenotype resembling that of *MpERF15*-overexpressing thalli, although less pronounced.

However, clear differences also exist. It has been demonstrated that *ERF115*'s stem cell activity can be strongly enhanced through its association with members of the GRAS family of TFs (42). This association is at least in part controlled by the presence of a conserved N-terminally located 11-amino acid sequence in *ERF115*. Although no direct interaction of *ERF109* with a GRAS TF has been reported, its protein sequence holds this conserved amino acid sequence motif, being characteristic for the ERF subfamily class X. In contrast, none of the *M. polymorpha* ERFs hold this N-terminal sequence, indicating that the ERF association with GRAS TFs might have emerged later during evolution, granting additional benefit or control over ERF activity.

A second major difference can be found downstream, because *MpERF15*, but not *ERF109*, appears to control oxylipin biosynthesis. Transcriptomic analyses of *Mperf15<sup>ko</sup>* and *MpERF15<sup>OE</sup>* thalli demonstrated that *MpERF15* drives the expression of the oxylipin biosynthesis genes *MpAOS2* and *MpAOC*, accompanied with an accumulation of dn-OPDA in *MpERF15<sup>OE</sup>* lines. After wounding, *Mperf15<sup>ko</sup>* lines displayed a reduced level of both OPDA and dn-OPDA compared to the WT. Moreover, we demonstrated that

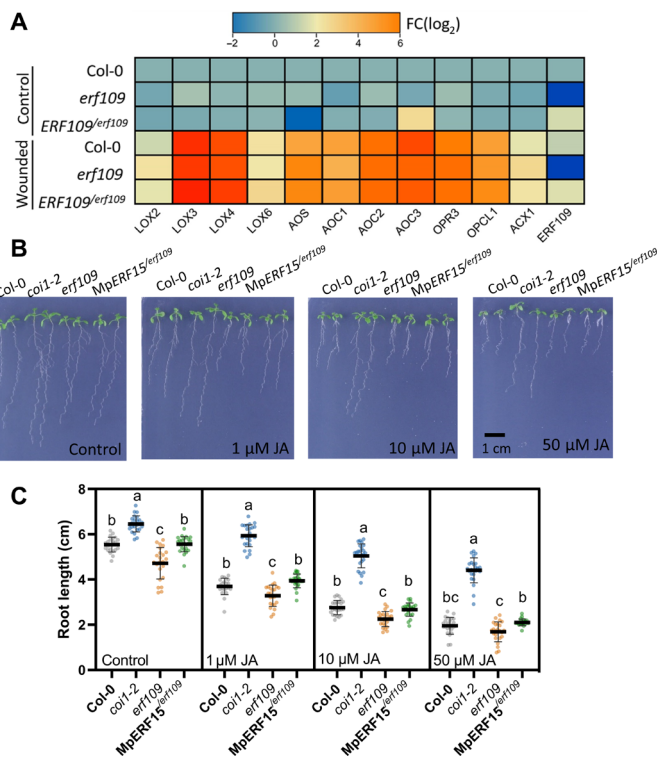


**Fig. 8. Arabidopsis ERF109 does not control jasmonate biosynthesis genes.** (A) Heatmap of RT-qPCR analysis of a subset of JA biosynthesis genes in Col-0, *erf109*, and *ERF109pro:ERF109erf109* lines of 14-day-old unwounded and wounded seedlings ( $n = 3$ , 15 seedlings per repeat), harvested 1 hour after wounding. The FC of expression levels was normalized with log<sub>2</sub> scale. Colors indicate up-regulated (red) and down-regulated genes (blue). (B) Five-day-old *Arabidopsis* Col-0, *coil-2*, *erf109*, and *ERF109pro:ERF109erf109* seedlings grown for 7 days on control medium (–) or medium supplemented with 1, 10, or 50 μM JA. Scale bar, 1 cm. (C) Quantification of root length of seedlings shown in (B). Data represent means ± SD. Dots represent individual data points ( $n > 22$ ). The different letters indicate significant differences (one-way ANOVA/post hoc Tukey HSD test,  $P < 0.01$ ) of each genotype.

accumulation of OPDA/dn-OPDA is essential for the regeneration process, because *Mper15<sup>ko</sup>* and *Mpaoc<sup>ko</sup>* mutants displayed a defect regeneration phenotype that could be rescued by OPDA application. In addition, *MpERF15<sup>OE</sup>* lines were hypersensitive to OPDA/dn-OPDA, probably due to an already higher endogenous dn-OPDA level, whereas *Mper15<sup>ko</sup>* appeared to be more resistant, both phenotypes that are shared with *MpMYC<sup>OE</sup>* and *Mpmyc* mutants, respectively (29). In contrast, *Arabidopsis* *ERF109* did not control the expression of JA biosynthesis genes, nor did *erf109* knockout plants display an altered sensitivity toward JA.

*Arabidopsis* MYC2 indirectly regulates the expression of JA biosynthetic genes by binding to the promoter of *OCTADECANOID-RESPONSIVE AP2/ERF-DOMAIN TRANSCRIPTION FACTOR 47* (*ORA47*), encoding an AP2/ERF subfamily class II member being only distantly related to ERF109 genes (45). *ORA47* itself controls the transcriptional activation of several JA biosynthetic genes (26, 45, 46). Likewise, tomato *SIERF15* and *SIERF16*, being *ORA47* homologs, control the expression of key JA biosynthesis genes, including *LOXD*, *AOC*, and *OPR3* (47). Similarly, the Chinese flowering cabbage *BrERF72* gene is MeJA inducible and directly activates the expression of *BrLOX4*, *BrAOC3*, and *BrOPR3* to regulate JA

production (48). Differently to ERF109 and MpERF15, the activity of these genes has not been linked with regeneration, but rather to leaf senescence (*BrERF72*), herbivory (*SIERF15* and *SIERF16*), salinity, low boron, and drought (*ORA47*) (45, 47, 48). These findings suggest that the genetic networks controlling JA biosynthesis might have been reshuffled during evolution. Thus, we hypothesize that MpERF15 evolved into ERF109 with most of its functions preserved, but lacking the ability to drive oxylipin biosynthesis, a function taken over by other ERF family members, including *ORA47*.

Although both the  $\alpha$ -linolenic acid and hexadecatrienoic acid pathways share the AOS and AOC proteins, transcriptional activation of MpAOS2 and MpAOC by MpERF15 in the *MpERF15<sup>OE</sup>* lines resulted in an increase in dn-OPDA, but not OPDA. Interestingly, whereas we found that the potentially upstream biosynthetic genes MpLOX1 and MpLOX4 are both wound inducible in an MpERF15-dependent manner (fig. S11, A and B), only MpLOX1 is transcriptionally induced in the *MpERF15<sup>OE</sup>* lines, whereas MpLOX4 is even repressed (fig. S11, C and D). Combined, these data may indicate that MpLOX1 and MpLOX4 are active in the dn-OPDA and OPDA biosynthetic pathway, respectively (Fig. 6D). Alternatively, under nonwounding conditions, OPDA may be difficult to detect because of rapid conversion to dn-OPDA (27).

Similarly to angiosperms, *M. polymorpha* OPDA/dn-OPDA biosynthesis is subjected to a positive feedback loop, because feeding of thalli with deuterated precursors results in the accumulation of nondeuterated OPDA and dn-OPDA isomers (27). Being an activator of dn-OPDA biosynthesis and operating downstream of MpCOI1, marks MpERF15 as an essential coordinator of this feedback loop, driving wound-induced oxylipin biosynthesis. Accordingly, we demonstrated the endogenous MpERF15 gene to be transcriptionally activated by the MpERF15 overexpression construct, and that the amplification loop is MpCOI1 dependent. Accordingly, transcriptional activation of the OPDA/dn-OPDA biosynthesis genes, as well as the cell division and apical notch phenotypes, is lost when MpERF15 is overexpressed in the *Mpcoil-2* mutant background. It suggests that, rather than solely MpERF15, it is the MpCOI1-MpERF15-OPDA/dn-OPDA feedback loop that is mainly accountable for the observed phenotypes. Although this feedback loop accounted for only a threefold up-regulation of MpERF15 transcription compared to the more than 100-fold increase in transcripts by the MpERF15<sup>OE</sup> construct, the latter triggered transcript accumulation in all thalli cells, including many that are likely not dn-OPDA responsive, whereas the increase of MpERF15 due to the feedback loop happens in responsive cells only.

Although MpERF15 appears to act as an amplifier of dn-OPDA biosynthesis, it may not be the initial trigger, as approximately 30% of the OPDA/dn-OPDA induced after wounding in Tak-1 plants could still be observed in the *Mper15<sup>ko</sup>* mutants. Thus, unknown, MpERF15-independent factors may be involved in the early up-regulation of wounding-induced OPDA/dn-OPDA.

Strikingly, compared to the WT, many genes displayed reduced expression in the *Mper15<sup>ko</sup>* plants under unwounded conditions. Although many of these were MpCOI1 responsive, we observed no pronounced phenotypes in unwounded *Mper15<sup>ko</sup>* thalli, neither a major impact on their metabolome. These data suggest no pronounced role for OPDA/dn-OPDA and MpCOI1 under control conditions, fitting with the absence of clear phenotypes of *Mpcoil-2* and *Mpmyc* mutants (27, 29, 38). These data indicate that MpERF15's role might be restricted to the wound response.

Next to ERF subfamily class X, other types of ERF TFs are also involved in regeneration in land plants. *WOUND INDUCED DEDIFFERENTIATION 1* (*WIND1*), encoding an ERF subfamily class I, is rapidly induced in response to wounding and promotes callus formation (49). *WIND1* activates the expression of ERF subfamily class VIIIb *ENHANCER OF SHOOT REGENERATION 1/DORNROSCHEN* (*ESR1/DRN*), whose overexpression induces cytokinin-independent shoot regeneration (50). In *M. polymorpha*, *MpERF20/LAXR*, the ortholog of *Arabidopsis* *ESR1*, was recently reported to be another regeneration-controlling ERF that is induced in basal cut thalli in response to a decrease in auxin, possibly due to a wounding-induced auxin drain (11). The transcriptional response of *MpERF20/LAXR* after wounding is relatively late, with no significant up-regulated expression at 1 hour after tissue incision, when *MpERF15* expression peaks, suggesting that *MpERF20/LAXR* might operate downstream of *MpERF15*. We observed a reduced induction of *MpERF20/LAXR* in *Mperfl5<sup>ko</sup>* (as well as *Mpcoi1-2* and *Mpaoc<sup>ko</sup>*) 12 hours after wounding, whereas its expression is induced in the *MpERF15<sup>OE</sup>* line. Future work requires a better understanding of the relationship between *MpERF15* and *MpERF20/LAXR*.

Although we demonstrated that the regeneration defect of *Mperfl5<sup>ko</sup>* thalli could be rescued by OPDA application, this rescue was highly dependent on the dose and duration of OPDA application, as prolonged OPDA and dn-OPDA application strongly affected thallus growth. This observation correlates with the only transient increase of *MpERF15* transcript levels after wounding, with a peak in expression at 1 hour after cutting, indicative for a role for *MpERF15* in only the early event of regeneration. After wounding, a reduction in the endogenous auxin level in *M. polymorpha* explants is observed, reaching a minimum level in the basal part at 3 hours after excision, after which the auxin levels recover (11), probably through de novo synthesis. *Arabidopsis* *ERF109* up-regulates the expression of the *ASA1* auxin biosynthesis genes within 2 hours of leaf detachment to promote rooting from leaf explants (19). Also, in *M. polymorpha*, *MpASA1* operates downstream of *MpERF15*, but is a slow responsive gene, with a slight up-regulation of *MpASA1* expression levels within 2 hours after wounding, whereas the *Mperfl5<sup>ko</sup>* mutant showed reduced *MpASA1* expression at 4 hours after wounding. It indicates that the *MpERF15*-induced *MpASA1* induction may contribute to the reestablishment of auxin levels after wounding. Together, it suggests a dual role of *MpERF15* in the regeneration response, with an early role in activating an *MpCOI1-MpERF15-OPDA/dn-OPDA* feedback loop in response to wound signals to generate a pulse of OPDA/dn-OPDA accumulation, followed by a potential role in activation of auxin biosynthesis to promote tissue regeneration.

To summarize, we show that *MpERF15* plays an essential role in tissue regeneration after wounding and that it drives oxylipin biosynthesis. It is tempting to speculate that oxylipins are not the only metabolites participating in the *MpERF15*-dependent wound response pathway in *M. polymorpha*. Next to OPDA and dn-OPDA, our untargeted metabolic analysis detected many compound ions to be sharply induced after wounding in an *MpERF15*-dependent manner. There is a possibility that they might participate in the regeneration process and are accountable for the observed effects on cell number and the number of apical notches following *MpERF15* overexpression. Moreover, *MpERF15* transcriptional induction after wounding is maintained in the *Mpcoi1-2* mutant background, albeit at a much lower absolute transcript level. This indicates that

*MpCOI1-OPDA/dn-OPDA* controls *MpERF15* expression levels, through the described positive feedback loop, but does not account for the wound inducibility of *MpERF15*. Gaining insights into the identity and function of the component both operating upstream of *MpERF15* and downstream of dn-OPDA might prove to be useful to improve the regeneration potential of recalcitrant species.

## MATERIALS AND METHODS

### Plant material and growth conditions

*M. polymorpha* accession Tak-1 was used as WT. The OpenPlant toolkit (51) was used to construct the *MpERF15* (Mp7g09350). The full length of the *MpERF15* open reading frame (ORF) region (2013 nucleotides) was cloned into the pDONR221 entry vector via the BP reaction (Invitrogen). To remove the *Bsa* I or *Sap* I restriction sites, site-directed mutagenesis was performed as previously described (52). To create the *MpERF15<sup>OE</sup>* lines, *MpERF15* was cloned into the pCsB (OP-006) vector via Gibson reaction and by subsequently recombining it via a loop assembly reaction behind the endogenous ELONGATION FACTOR 1 $\alpha$  (*MpEF1 $\alpha$* , Mp3g23400) promoter and in front of pCsC\_spacer (OP-015), pCsC\_GR, and 3TERM\_Nos-35S (OP-054) in the pCk2 (OP-002) vector. The *proMpEF1 $\alpha$ :MpERF15<sup>OE</sup>* construct was created by recombining L1\_HyR-Ck1 (OP-063), pCk2\_MpERF15<sup>OE</sup>, pCk3\_ *proMpEF1 $\alpha$ :Tdtomato-N7* (or L1\_UBE2:mT-N7-Ck3 OP-066), and pCk4\_spacer (OP-012) (or L1\_UBE2:mS-Lt-Ck4 OP-070) via a loop assembly reaction into the pCsA (OP-005) vector. The *proMpEF1 $\alpha$ :MpERF15<sup>GR</sup>* construct was created by recombining L1\_HyR-Ck1 (OP-063), pCk2\_MpERF15<sup>GR</sup>, L1\_UBE2:mT-N7-Ck3 (OP-066), and L1\_UBE2:mS-Lt-Ck4 (OP-070) via a loop assembly reaction into the pCsC (OP-007) vector. For *proMpYUC2:GUS*, *MpYUC2pro\_pENTR/D-TOPO* was subcloned into the pMpGWB304 vector by LR reaction (Invitrogen). For *ERF109<sup>OE</sup>* (*pro35S:ERF109*), the plasmid pDONR221 carrying *ERF109* was already available in the laboratory, and *ERF109\_pDONR221* was cloned into the pMpGWB130 vector by LR reaction. *Agrobacterium*-mediated *M. polymorpha* transformation was performed as previously described (10). Transformants were selected onto medium containing hygromycin (10 mg/liter) or 0.5  $\mu$ M chlorsulfuron and cefotaxime (100  $\mu$ g/ml), and G1 generation plants were selected to perform the experiments.

Two constructs were made for use in the cross-species complementation assay using gateway cloning technology: *ERF109pro:ERF109* and *ERF109pro:MpERF15*. The 3168-nucleotide promoter region upstream of the *ERF109* start codon was cloned into the pDONR4P1R entry vector via the BP reaction (Invitrogen). *ERF109pro\_pDONR4P1R* and *MpERF15\_pDONR221* or *ERF109\_pDONR221* resulting vectors were cloned into pK7m24GW,3 destination vectors via LR reaction to obtain the respective constructs. Then, the constructs were introduced into the *A. thaliana* *erf109* mutant by *Agrobacterium*-mediated floral dipping, primary transformants were selected on 0.5 Murashige and Skoog agar plates containing kanamycin antibiotics (35  $\mu$ g/ml), and T3 homozygous plants were selected to perform the experiments.

For the yeast two-hybrid experiment, *MpJAZ* sequences were amplified from Tak-1 complementary DNA (cDNA) and cloned into pDONR221 through the BP reaction. The pDONR221 plasmids carrying AtJAZ3, AtJAZ4, and AtJAZ9 were already available in the laboratory. Through the LR reaction, *MpERF15* and *AtERF109* were cloned into pDEST22; *MpJAZ*, AtJAZ3, AtJAZ4, and AtJAZ9 were cloned into pDEST32.

*M. polymorpha* plants were cultured on half-strength (0.5) Gamborg's B5 medium (Duchefa Biochemie) with 1% (w/v) plant agar at 21°C under continuous white light (50 to 60  $\mu\text{mol m}^{-2} \text{s}^{-1}$ ). *Arabidopsis* seeds were sterilized in 70% ethanol for 10 min and subsequently sterilized with 4% NaClO<sub>3</sub> for 15 min, after which they were washed in sterile water for three times. For all experiments, the seeds were stratified in the dark for 2 days at 4°C before being placed in the growth room. Plants were grown in vitro under long-day conditions (16-hour light/8-hour dark) at 21°C on solidified 0.5 Murashige and Skoog medium (2.151 g/liter), sucrose (10 g/liter), and MES (0.5 g/liter), adjusted to pH 5.7 with 1 M KOH and agar (10 g/liter). For analysis of regeneration phenotypes, plants were grown vertically.

### Gene identification and phylogenetic analyses

Protein sequences were obtained from Genome Database for *M. polymorpha* (<https://marchantia.info>) and PLAZA 5.0 (<https://bioinformatics.psb.ugent.be/plaza/>) (53). The conserved AP2 domain was annotated with the National Center for Biotechnology Information (NCBI) conserved domain database ([www.ncbi.nlm.nih.gov/Structure/bwrpsb/bwrpsb.cgi](http://www.ncbi.nlm.nih.gov/Structure/bwrpsb/bwrpsb.cgi)). The phylogenetic analysis of the *A. thaliana* subfamily X and *M. polymorpha* ERFs was based on the N-terminal sequences including the conserved AP2 domain. The phylogenetic tree was constructed using the neighbor-joining method (p-distance, 1000 bootstrap iterations) with Mega software (v7.0), based on a multiple sequence alignment (generated with Clustal Omega) and trimming.

### CRISPR mutant generation

The established CRISPR-Cas9-mediated mutagenesis system in *M. polymorpha* was used to generate MpERF15 and MpAOC mutant lines (51). Two different guide RNAs (gRNAs) specific for MpERF15 and four different gRNAs specific for MpAOC (see table S1 for primers) were selected using the CRISPR direct web tool (<https://crispr.dbcls.jp>) based on the expected cut site in the beginning of the gene and minimal off-target scores, respectively. The gRNA1 and gRNA2 (gRNA3 and gRNA4) primer pairs were inserted into the L1\_lacZgRNA-Ck2 (OP-075) and L1\_lacZgRNA-Ck3 (OP-074) vectors, respectively, after which these were recombined with the L1\_CsR-Ck1 (OP-062) and L1\_Cas9-Ck4 (OP-073) vectors into the pCsA (OP-005) acceptor plasmid using Golden Gate Loop Assembly according to the manufacturer's recommendations (51). The construct was transformed into Tak-1 background plants, and transformants were selected with 0.5  $\mu\text{M}$  chlorsulfuron and cefotaxime (100  $\mu\text{g/ml}$ ). Mutant lines were genotyped by PCR (table S1); fully frame-shifted transgenic lines were selected for further experiments.

### Confocal microscopy

To stain the *M. polymorpha* cell walls, 0-day-old gemmae were mounted in a 10  $\mu\text{M}$  propidium iodide (PI) solution as previously described (excitation, 488 nm; emission, 555 to 600 nm) (54), or 0-day-old gemmae were treated by ClearSee protocol (55) and 0.1% calcofluor white (excitation, 405 nm; emission, 415 to 443 nm) dissolved in ClearSee was used for 1 hour with vacuuming and imaged using a Zeiss LSM 710 confocal microscope. The confocal images were made binary (black and white), and the gemmaling size was measured using the wand tool in ImageJ. For *M. polymorpha* gemmaling cell number, confocal images were analyzed in ImageJ running a macro script from The BioVoxel Image Processing and Analysis Toolbox, as previously described (56). To observe fluorescence, excitation at 561 nm and emission at 570 to 600 nm were used for

tdTomato, and excitation at 405 nm and emission at 460 to 485 nm were used for mTurquoise2.

### EdU staining

Cell cycle activity was visualized using the Click-iT EdU Imaging Kit (Thermo Fisher Scientific) according to the manufacturer's instruction and a method described previously with some modifications (8). Zero-day-old gemmae were transferred to a microplate containing 0.5 Gamborg's B5 liquid medium with 20  $\mu\text{M}$  EdU for 24 hours. Incorporation of EdU was terminated by fixing gemmalings with 4% paraformaldehyde (PFA) solution in 1 $\times$  PME [50 mM Pipes (pH 6.9), 5 mM MgSO<sub>4</sub>, and 1 mM EGTA]. After washing with phosphate-buffered saline (PBS) three times and then permeabilization with 0.5% Triton X-100 in PBS for 30 min, EdU incorporated into DNA was stained by incubation in the dark with Alexa Fluor 488-azide-containing Click-iT reaction cocktail for 1 hour. After washing successively with PBS containing 3% bovine serum albumin and PBS, gemmalings were treated by ClearSee overnight and the cell wall was stained by 0.1% calcofluor white.

### Regeneration assays

For the 2-day-old gemmaling apical notch excision regeneration experiment, gemmalings were isolated from the gemma cups and cultured in a liquid 0.5 Gamborg's B5 medium supplemented with MES (0.5 g/liter, pH 5.7) for 2 days. Under a microscope, the two apical notches were excised with a sterile blade; the gemmalings were kept away from drought and heat by pouring 0.5 B5 medium on the surface. The gemmalings were cultured further on 0.5 B5 medium with 1% (w/v) agar, and pictures were taken daily to observe and determine regeneration size by ImageJ. Regeneration was calculated by plotting the ratio of 4 days post-cut (dpc) minus 0 dpc to 0 dpc explant sizes [(4 dpc - 0 dpc)/0 dpc]. If the ratio is 1, this means that the size of the regenerated tissue is equal to the size of the original explant at 0 dpc. For the OPDA rescue experiment, meristematic-removed gemmalings were transferred on 0.5 B5 medium 1% (w/v) agar plates with 10 nM OPDA or EtOH (control) for 2 hours, after which they were transferred to normal 0.5 B5 medium. Ten-day-old basal explant regeneration experiment was performed as described previously (11). Regeneration was calculated by plotting the ratio of 8 dpc minus 0 dpc to 0 dpc explant sizes [(8 dpc - 0 dpc)/0 dpc]. The *Arabidopsis* de novo root regeneration experiment was performed as described previously (19). Stringent root tip cutting was performed at a 200- $\mu\text{m}$  distance from the 7-day-old seedling root tip, as described previously (57). Root tip regeneration 72 hours after cutting was scored as negative when collapse of the root meristem was observed.

### RT-qPCR analysis

RNA was isolated with the RNeasy Mini Kit (Qiagen), treated on-column with the RQ1 RNase-Free DNase (Promega), and used for cDNA synthesis with the iScript cDNA Synthesis Kit (Bio-Rad). RT-qPCR was performed using the SYBR Green Kit (Roche) with 100 nM primers and 0.125  $\mu\text{l}$  of RT reaction product in a total volume of 5  $\mu\text{l}$  per reaction. Reactions were run and analyzed on LightCycler 480 (Roche) according to the manufacturer's instructions. For *M. polymorpha*, MpEF1 $\alpha$  (Mp3g23400) and MpActin (Mp6g11010) were used as reference genes for normalization (58). Every experiment was performed using three biological replicates, holding six plants per replicate. For MpERF15 5'UTR, primers amplified the 49-base pair (bp) fragment from nucleotides -255 to -207 in the 5'UTR, and for

Mp*ERF15* 3'UTR, primers amplified the 46-bp fragment from nucleotides 2312 to 2357 in the 3'UTR. For *Arabidopsis*, *PAC1* and *RPS26C* were used as reference genes for normalization. For each reaction, three technical repeats were performed. qPCR data were analyzed using the  $2^{-\Delta\Delta Ct}$  method. Primer sequences can be found in table S1.

### RNA-seq analysis

WT Tak-1 and three independent transgenic *Mperfl5<sup>ko</sup>* (#9, #10, and #13) were cultured on 0.5 Gamborg's B5 agar medium for 14 days. Three biological replicates formed by 12 plants per replicate were harvested from Tak-1 or *Mperfl5<sup>ko</sup>* with and without wounding for 1 hour and placed in a 2-ml tube containing beads. These samples were frozen with liquid nitrogen and crushed by shaking the tube at 2000 rpm for 1 min. Total RNA was extracted using the RNeasy Plant Mini Kit (Qiagen), and Illumina Tru-Seq libraries were generated from cDNA and sequenced on a NextSeq500 100-bp single-end run. All analyses were done using the Galaxy platform. Reads were filtered and trimmed, after which transcript quantification was performed by Salmon version 0.7.2 (59) using the *M. polymorpha* reference genome MpTak1v5.1 (13), with all parameters set to default values. Transcript quantification results generated by Salmon were corrected for gene length variations across the samples using the tximport 1.6.0 R package (60) and were further analyzed using the DESeq2 package (61). The magnitude of the fluctuation in expression was calculated as  $\log_2$  (fold change), and using DESeq2, multiplicity correction was applied by the Benjamini-Hochberg method on the *P* values to control the false discovery rate (FDR). We considered genes with  $\log_2$  ratios greater than 1 or less than -1 and expected FDR of <5% as differentially expressed for Tak-1 wounded versus unwounded and *Mperfl5<sup>ko</sup>* unwounded versus Tak-1 unwounded. For *Mperfl5<sup>ko</sup>* wounded versus Tak-1 wounded, we considered genes with  $\log_2$  ratios less than -0.4 and expected FDR of <5% as down-regulated genes. GO analysis was performed using TBtools (62). In this tool, GO annotations for MpTak1v5.1\_r1 genes (13) with some modification were used and GO terms with corrected *P* < 0.05 were considered significantly enriched. RNA-seq raw data from this study were deposited in Gene Expression Omnibus (accession number: GSE196912).

### Untargeted metabolomics

For the wounding response experiment, five biological replicates formed by 12 plants per replicate were harvested from 14-day-old WT Tak-1, *Mperfl5<sup>ko</sup>*, and *MpERF15<sup>OE</sup>* with and without wounding for 1 hour, placed in a 2-ml tube containing beads, and frozen immediately in liquid nitrogen. Then, the tissue was extracted by shaking at 2000 rpm for 15 min with 1 ml of methanol. After centrifugation, the supernatant was transferred to new 1.5-ml tubes and vacuum-dried. Subsequently, the pellet was resuspended in equal volumes of cyclohexane and ultrapure water [100  $\mu$ l (v/v)]. After vortexing, samples were centrifuged, and 10  $\mu$ l of the aqueous phase was injected on the Waters Acquity Ultraperformance Liquid Chromatography System coupled to a Waters Vion-IMS-QTOF (Ion Mobility Spectrometry Quadrupole Time-of-flight) mass spectrometer (MS) equipped with an ESI source operating in negative (ESI-) or positive (ESI+) ionization mode. Chromatographic separation was done by reverse phase (BEH C18 column, 150  $\times$  2.1 mm, 2.1  $\mu$ m), and column temperature was maintained at 40°C. A gradient of two buffers was used: buffer A (99:1:0.1 water:acetonitrile:formic acid, pH 3) and buffer B (99:1:0.1 acetonitrile:water:formic acid, pH 3), as

follows: 99% A for 0.1 min decreased to 50% A in 30 min, decreased to 30% in 5 min, decreased to 0% in 2 min. The flow rate was set to 0.35 ml min<sup>-1</sup>. For MS detection, the LockSpray ion source was operated in positive or negative ESI mode under the following specific conditions: capillary voltage, 3 kV for negative, 2.5 kV for positive; reference capillary voltage, 3 kV; source temperature, 120°C; desolvation gas temperature, 550°C; desolvation gas flow, 800 liters hour<sup>-1</sup>; and cone gas flow, 50 liters hour<sup>-1</sup>. Mass range was set from 50 to 1500 Da. The collision energy for full MSe was set at 6 eV (low energy) and ramped from 20 to 70 eV (high energy), and intelligent data capture intensity threshold was set at 5. For data-dependent acquisition (DDA)-MS/MS, the low mass ramp was ramped between 20 and 40 eV, and the high mass ramp was ramped between 40 and 80 eV. Nitrogen (greater than 99.5%) was used as desolvation and cone gas. Leucin-enkephalin [250 pg  $\mu$ l<sup>-1</sup> solubilized in water:acetonitrile 1:1 (v/v), with 0.1% formic acid] was used for the lock mass calibration, with scanning every 2 min at a scan time of 0.1 s. Profile data were recorded through the UNIFI Scientific Information System (Waters). Data processing (compound ion detection, alignment, and normalization) was performed with Progenesis Q1 software version 2.4 (Waters). Pooled samples were included for data alignment purposes, system reproducibility, and DDA-MS/MS generation. Quality control samples were included for retention time and mass accuracy stability monitoring during sample analysis. All biological samples were analyzed at random, and for every sample, a unique "chromatogram" was generated (= raw data). To compensate for the exact amount of plant material that was extracted for each sample, a normalization was performed for all compound ions based on the dry weight of each sample. PCA was done on *glog* transformed and autoscaled features through MetaboAnalyst 5.0 (63). The number of compound ions was considered to be different based on Student's *t* test analysis (*P* < 0.001) and a more than twofold change in abundance. All compound ions were matched against external (spectral) databases (including PlantCyC, NPAtlas, and NIST20 MSMS). For phytohormone identification and comparative quantification, OPDA and dn-OPDA were further confirmed through authentic standards (OPDA: Cayman, no. 88520; dn-OPDA: Cayman, no. 10710).

### Yeast two-hybrid assay

The yeast two-hybrid assay was performed as described previously (64). Briefly, plasmids encoding the bait (pDEST32) and prey (pDEST22) were transformed into the yeast strain PJ69-4 $\alpha$ , and interactions between proteins were assayed by the mating method.

### GUS staining

Plants were grown for the indicated period and fixed in an ice-cold 80% acetone solution for 3 hours. Samples were washed three times with phosphate buffer (14 mM NaH<sub>2</sub>PO<sub>4</sub> and 36 mM Na<sub>2</sub>HPO<sub>4</sub>) before being incubated in staining buffer [5-bromo-4-chloro-3-indolyl- $\beta$ -D-glucuronic acid (0.5 mg/ml), potassium ferricyanide (0.165 mg/ml), potassium ferrocyanide (0.211 mg/ml), EDTA (0.585 mg/ml; pH 8), and 0.1% (v/v) Triton-X100, dissolved in phosphate buffer] at 37°C between 30 min and 16 hours until sufficient staining was observed.

### SUPPLEMENTARY MATERIALS

Supplementary material for this article is available at <https://science.org/doi/10.1126/sciadv.abo7737>

[View/request a protocol for this paper from Bio-protocol.](#)

## REFERENCES AND NOTES

- P. Marhava, L. Hoermayer, S. Yoshida, P. Marhavý, E. Benková, J. Friml, Re-activation of stem cell pathways for pattern restoration in plant wound healing. *Cell* **177**, 957–969.e13 (2019).
- J. Heyman, B. Canher, A. Bisht, F. Christiaens, L. De Veylder, Emerging role of the plant ERF transcription factors in coordinating wound defense responses and repair. *J. Cell Sci.* **131**, jcs208215 (2018).
- M. Ikeuchi, D. S. Favero, Y. Sakamoto, A. Iwase, D. Coleman, B. Rymen, K. Sugimoto, Molecular mechanisms of plant regeneration. *Annu. Rev. Plant Biol.* **70**, 377–406 (2019).
- M. Ikeuchi, Y. Ogawa, A. Iwase, K. Sugimoto, Plant regeneration: Cellular origins and molecular mechanisms. *Development* **143**, 1442–1451 (2016).
- F. Bannoud, C. Bellini, Adventitious rooting in *Populus* species: Update and perspectives. *Front. Plant Sci.* **12**, 668837 (2021).
- M. Nagle, A. Déjardin, G. Pilate, S. H. Strauss, Opportunities for innovation in genetic transformation of forest trees. *Front. Plant Sci.* **9**, 1443 (2018).
- C. Díaz-Sala, Molecular dissection of the regenerative capacity of forest tree species: Special focus on conifers. *Front. Plant Sci.* **9**, 1943 (2019).
- R. Nishihama, K. Ishizaki, M. Hosaka, Y. Matsuda, A. Kubota, T. Kohchi, Phytochrome-mediated regulation of cell division and growth during regeneration and sporeling development in the liverwort *Marchantia polymorpha*. *J. Plant Res.* **128**, 407–421 (2015).
- M. Ishikawa, T. Murata, Y. Sato, T. Nishiyama, Y. Hiwataishi, A. Imai, M. Kimura, N. Sugimoto, A. Akita, Y. Oguri, W. E. Friedman, M. Hasebe, M. Kubo, Physcomitrella cyclin-dependent kinase a links cell cycle reactivation to other cellular changes during reprogramming of leaf cells. *Plant Cell* **23**, 2924–2938 (2011).
- A. Kubota, K. Ishizaki, M. Hosaka, T. Kohchi, Efficient agrobacterium-mediated transformation of the liverwort *Marchantia polymorpha* using regenerating thalli. *Biosci. Biotechnol. Biochem.* **77**, 167–172 (2013).
- S. Ishida, H. Suzuki, A. Iwaki, S. Kawamura, S. Yamaoka, M. Kojima, Y. Takebayashi, K. Yamaguchi, S. Shigenobu, H. Sakakibara, T. Kohchi, R. Nishihama, Diminished auxin signaling triggers cellular reprogramming by inducing a regeneration factor in the liverwort *Marchantia polymorpha*. *Plant Cell Physiol.* **63**, 384–400 (2022).
- J. L. Bowman, T. Kohchi, K. T. Yamato, J. Jenkins, S. Shu, K. Ishizaki, S. Yamaoka, R. Nishihama, Y. Nakamura, F. Berger, C. Adam, S. S. Aki, F. Althoff, T. Araki, M. A. Arteaga-Vazquez, S. Balasubramanian, K. Barry, D. Bauer, C. R. Boehm, L. Briginshaw, J. Caballero-Perez, B. Catarino, F. Chen, S. Chiyoda, M. Chovatia, K. M. Davies, M. Delmans, T. Demura, T. Dierschke, L. Dolan, A. E. Dorantes-Acosta, D. M. Eklund, S. N. Florent, E. Flores-Sandoval, A. Fujiyama, H. Fukuzawa, B. Galik, D. Grimaneli, J. Grimwood, U. Grossniklaus, T. Hamada, J. Haseloff, A. J. Hetherington, A. Higo, Y. Hirakawa, H. N. Hundley, Y. Ikeda, K. Inoue, S. I. Inoue, S. Ishida, Q. Jia, M. Kakita, T. Kanazawa, Y. Kawai, T. Kawashima, M. Kennedy, K. Kinose, T. Kinoshita, Y. Kohara, E. Koide, K. Komatsu, S. Kopsischke, M. Kubo, J. Kyoizuka, U. Lagercrantz, S. S. Lin, E. Lindquist, A. M. Lipzen, C. W. Lu, E. de Luna, R. A. Martienssen, N. Minamino, M. Mizutani, M. Mizutani, M. Mochizuki, I. Monte, R. Mosher, H. Nagasaki, H. Nakagami, S. Naramoto, K. Nishitani, M. Ohtani, T. Okamoto, M. Okumura, J. Phillips, B. Pollak, A. Reinders, M. Rövekamp, R. Sano, S. Sawa, M. W. Schmid, M. Shirakawa, R. Solano, A. Spunde, N. Suetsugu, S. Sugano, A. Sugiyama, R. Sun, Y. Suzuki, M. Takenaka, D. Takezawa, H. Tomogane, M. Tsuzuki, T. Ueda, M. Umeda, J. M. Ward, Y. Watanabe, K. Yazaki, R. Yokoyama, Y. Yoshitake, I. Yotsui, S. Zachgo, J. Schmutz, Insights into land plant evolution garnered from the *Marchantia polymorpha* genome. *Cell* **171**, 287–304.e15 (2017).
- S. A. Montgomery, Y. Tanizawa, B. Galik, N. Wang, T. Ito, T. Mochizuki, S. Akimcheva, J. L. Bowman, V. Cognat, L. Maréchal-Drouard, H. Ekker, S. F. Hong, T. Kohchi, S. S. Lin, L. Y. D. Liu, Y. Nakamura, L. R. Valeeva, E. V. Shakhov, D. E. Shippen, W. L. Wei, M. Yagura, S. Yamaoka, K. T. Yamato, C. Liu, F. Berger, Chromatin organization in early land plants reveals an ancestral association between H3K27me3, transposons, and constitutive heterochromatin. *Curr. Biol.* **30**, 573–588.e7 (2020).
- M. Shimamura, *Marchantia polymorpha*: Taxonomy, phylogeny and morphology of a model system. *Plant Cell Physiol.* **57**, 230–256 (2016).
- H. Kato, M. Kouno, M. Takeda, H. Suzuki, K. Ishizaki, R. Nishihama, T. Kohchi, The roles of the sole activator-type auxin response factor in pattern formation of *Marchantia polymorpha*. *Plant Cell Physiol.* **58**, 1642–1651 (2017).
- K. Sugimoto, H. Temman, S. Kadokura, S. Matsunaga, To regenerate or not to regenerate: Factors that drive plant regeneration. *Curr. Opin. Plant Biol.* **47**, 138–150 (2019).
- W. Zhou, J. L. Lozano-Torres, I. Biloux, X. Zhang, Q. Zhai, G. Smant, C. Li, B. Scheres, A jasmonate signaling network activates root stem cells and promotes regeneration. *Cell* **177**, 942–956.e14 (2019).
- B.-B. Ye, G. D. Shang, Y. Pan, Z. G. Xu, C. M. Zhou, Y. B. Mao, N. Bao, L. Sun, T. Xu, J. W. Wang, AP2/ERF transcription factors integrate age and wound signals for root regeneration. *Plant Cell* **32**, 226–241 (2020).
- G. Zhang, F. Zhao, L. Chen, Y. Pan, L. Sun, N. Bao, T. Zhang, C. X. Cui, Z. Qiu, Y. Zhang, L. Yang, L. Xu, Jasmonate-mediated wound signalling promotes plant regeneration. *Nat. Plants* **5**, 491–497 (2019).
- X.-T. Cai, P. Xu, P. X. Zhao, R. Liu, L. H. Yu, C. B. Xiang, *Arabidopsis* ERF109 mediates cross-talk between jasmonic acid and auxin biosynthesis during lateral root formation. *Nat. Commun.* **5**, 5833 (2014).
- G.-Z. Han, Evolution of jasmonate biosynthesis and signaling mechanisms. *J. Exp. Bot.* **68**, 1323–1331 (2017).
- G. A. Howe, I. T. Major, A. J. Koo, Modularity in jasmonate signaling for multistress resilience. *Annu. Rev. Plant Biol.* **69**, 387–415 (2018).
- F. Zhang, J. Yao, J. Ke, L. Zhang, V. Q. Lam, X. F. Xin, X. E. Zhou, J. Chen, J. Brunzelle, P. R. Griffin, M. Zhou, H. E. Xu, K. Melcher, S. Y. He, Structural basis of JAZ repression of MYC transcription factors in jasmonate signalling. *Nature* **525**, 269–273 (2015).
- A. Chini, S. Gimenez-Ibanez, A. Goossens, R. Solano, Redundancy and specificity in jasmonate signalling. *Curr. Opin. Plant Biol.* **33**, 147–156 (2016).
- C. Zhang, Y. Lei, C. Lu, L. Wang, J. Wu, MYC2, MYC3, and MYC4 function additively in wounding-induced jasmonic acid biosynthesis and catabolism. *J. Integr. Plant Biol.* **62**, 1159–1175 (2020).
- A. Van Moerkercke, O. Duncan, M. Zander, J. Šimura, M. Broda, R. V. Bossche, M. G. Lewsey, S. Lama, K. B. Singh, K. Ljung, J. R. Ecker, A. Goossens, A. H. Millar, O. Van Aken, A MYC2/MYC3/MYC4-dependent transcription factor network regulates water spray-responsive gene expression and jasmonate levels. *Proc. Natl. Acad. Sci. U.S.A.* **116**, 23345–23356 (2019).
- I. Monte, S. Ishida, A. M. Zamarreño, M. Hamberg, J. M. Franco-Zorrilla, G. García-Casado, C. Gouhier-Darimont, P. Reymond, K. Takahashi, J. M. García-Mina, R. Nishihama, T. Kohchi, R. Solano, Ligand-receptor co-evolution shaped the jasmonate pathway in land plants. *Nat. Chem. Biol.* **14**, 480–488 (2018).
- C. Wasternack, B. Hause, A bypass in jasmonate biosynthesis – The OPR3-independent formation. *Trends Plant Sci.* **23**, 276–279 (2018).
- M. Peñuelas, I. Monte, F. Schweizer, A. Vallat, P. Reymond, G. García-Casado, J. M. Franco-Zorrilla, R. Solano, Jasmonate-related MYC transcription factors are functionally conserved in *Marchantia polymorpha*. *Plant Cell* **31**, 2491–2509 (2019).
- Y. Yamamoto, J. Ohshika, T. Takahashi, K. Ishizaki, T. Kohchi, H. Matusuura, K. Takahashi, Functional analysis of allene oxide cyclase, MpAOC, in the liverwort *Marchantia polymorpha*. *Phytochemistry* **116**, 48–56 (2015).
- A. Dave, I. A. Graham, Oxylipin signaling: A distinct role for the jasmonic acid precursor *cis*-(+)-12-oxo-phytodienoic acid (*cis*-OPDA). *Front. Plant Sci.* **3**, 42 (2012).
- T. Jing, R. Ardiansyah, Q. Xu, Q. Xing, R. Müller-Xing, Reprogramming of cell fate during root regeneration by transcriptional and epigenetic networks. *Front. Plant Sci.* **11**, 317 (2020).
- F. Christiaens, B. Canher, F. Lanssens, A. Bisht, S. Stael, L. de Veylder, J. Heyman, Pars pro toto: Every single cell matters. *Front. Plant Sci.* **12**, 656825 (2021).
- I. Monte, J. M. Franco-Zorrilla, G. García-Casado, A. M. Zamarreño, J. M. García-Mina, R. Nishihama, T. Kohchi, R. Solano, A single JAZ repressor controls the jasmonate pathway in *Marchantia polymorpha*. *Mol. Plant* **12**, 185–198 (2019).
- G. Soriano, S. Kneeshaw, G. Jimenez-Aleman, Á. M. Zamarreño, J. M. Franco-Zorrilla, M. F. Rey-Stolle, C. Barbas, J. M. García-Mina, R. Solano, An evolutionarily ancient fatty acid desaturase is required for the synthesis of hexadecatrienoic acid, which is the main source of the bioactive jasmonate in *Marchantia polymorpha*. *New Phytol.* **233**, 1401–1413 (2021).
- D. M. Eklund, K. Ishizaki, E. Flores-Sandoval, S. Kikuchi, Y. Takebayashi, S. Tsukamoto, Y. Hirakawa, M. Nonomura, H. Kato, M. Kouno, R. P. Bhalerao, U. Lagercrantz, H. Kasahara, T. Kohchi, J. L. Bowman, Auxin produced by the indole-3-pyruvic acid pathway regulates development and gemmae dormancy in the liverwort *Marchantia polymorpha*. *Plant Cell* **27**, 1650–1669 (2015).
- G. Takahashi, S. Betsuyaku, N. Okuzumi, T. Kiyosue, An evolutionarily conserved coreceptor gene is essential for CLAVATA signaling in *Marchantia polymorpha*. *Front. Plant Sci.* **12**, 657548 (2021).
- I. Monte, S. Kneeshaw, J. M. Franco-Zorrilla, A. Chini, A. M. Zamarreño, J. M. García-Mina, R. Solano, An ancient COI1-independent function for reactive electrophilic oxylipins in thermotolerance. *Curr. Biol.* **30**, 962–971.e963 (2020).
- S. Xiao, L. Dai, F. Liu, Z. Wang, W. Peng, D. Xie, COS1: An Arabidopsis coronatine insensitive1 suppressor essential for regulation of jasmonate-mediated plant defense and senescence. *Plant Cell* **16**, 1132–1142 (2004).
- O. Lorenzo, J. M. Chico, J. J. Sanchez-Serrano, R. Solano, JASMONATE-INSENSITIVE1 encodes a MYC transcription factor essential to discriminate between different jasmonate-regulated defense responses in *Arabidopsis*. *Plant Cell* **16**, 1938–1950 (2004).
- B. Canher, F. Lanssens, A. Zhang, A. Bisht, S. Mazumdar, J. Heyman, F. Augstein, S. Wolf, A. Carlsbecker, C. W. Melnyk, L. De Veylder, The regeneration factors ERF114 and ERF115 act as transducers of mechanical cues to developmental pathways. *bioRxiv* 2021.11.29.470368 [Preprint]. 30 November 2021. <https://doi.org/10.1101/2021.11.29.470368>.
- J. Heyman, T. Cools, B. Canher, S. Shavialenka, J. Traas, I. Vercauteren, H. van den Daele, G. Persiau, G. de Jaeger, K. Sugimoto, L. de Veylder, The heterodimeric transcription factor complex ERF115-PAT1 grants regeneration competence. *Nat. Plants* **2**, 16165 (2016).

43. J. Heyman, T. Cools, F. Vandenbussche, K. S. Heyndrickx, J. van Leene, I. Vercauteren, S. Vanderauwera, K. Vandepoele, G. de Jaeger, D. van der Straeten, L. de Veylder, ERF115 controls root quiescent center cell division and stem cell replenishment. *Science* **342**, 860–863 (2013).
44. B. Canher, J. Heyman, M. Savina, A. Devendran, T. Eekhout, I. Vercauteren, E. Prinsen, R. Matosevich, J. Xu, V. Mironova, L. de Veylder, Rocks in the auxin stream: Wound-induced auxin accumulation and ERF115 expression synergistically drive stem cell regeneration. *Proc. Natl. Acad. Sci. U.S.A.* **117**, 16667–16677 (2020).
45. H.-Y. Chen, E. J. Hsieh, M. C. Cheng, C. Y. Chen, S. Y. Hwang, T. P. Lin, ORA47 (octadecanoid-responsive AP2/ERF-domain transcription factor 47) regulates jasmonic acid and abscisic acid biosynthesis and signaling through binding to a novel cis-element. *New Phytol.* **211**, 599–613 (2016).
46. R. Hickman, M. C. van Verk, A. J. H. van Dijken, M. P. Mendes, I. A. Vroegop-Vos, L. Caarls, M. Steenbergen, I. van der Nagel, G. J. Wesselink, A. Jironkin, A. Talbot, J. Rhodes, M. de Vries, R. C. Schuurink, K. Denby, C. M. J. Pieterse, S. C. M. van Wees, Architecture and dynamics of the jasmonic acid gene regulatory network. *Plant Cell* **29**, 2086–2105 (2017).
47. C. Hu, C. Wei, Q. Ma, H. Dong, K. Shi, Y. Zhou, C. H. Foyer, J. Yu, Ethylene response factors 15 and 16 trigger jasmonate biosynthesis in tomato during herbivore resistance. *Plant Physiol.* **185**, 1182–1197 (2021).
48. X.-I. Tan, Z. Q. Fan, W. Shan, X. R. Yin, J. F. Kuang, W. J. Lu, J. Y. Chen, Association of BrERF72 with methyl jasmonate-induced leaf senescence of Chinese flowering cabbage through activating JA biosynthesis-related genes. *Hortic. Res.* **5**, 22 (2018).
49. A. Iwase, N. Mitsuda, T. Koyama, K. Hiratsua, M. Kojima, T. Arai, Y. Inoue, M. Seki, H. Sakakibara, K. Sugimoto, M. Ohme-Takagi, The AP2/ERF transcription factor WIND1 controls cell dedifferentiation in Arabidopsis. *Curr. Biol.* **21**, 508–514 (2011).
50. A. Iwase, H. Harashima, M. Ikeuchi, B. Rymen, M. Ohnuma, S. Komaki, K. Morohashi, T. Kurata, M. Nakata, M. Ohme-Takagi, E. Grotewold, K. Sugimoto, WIND1 promotes shoot regeneration through transcriptional activation of ENHANCER OF SHOOT REGENERATION1 in Arabidopsis. *Plant Cell* **29**, 54–69 (2017).
51. S. Sauret-Güeto, E. Frangedakis, L. Silvestri, M. Rebmann, M. Tomaselli, K. Markel, M. Delmans, A. West, N. J. Patron, J. Haseloff, Systematic tools for reprogramming plant gene expression in a simple model, *Marchantia polymorpha*. *ACS Synth. Biol.* **9**, 864–882 (2020).
52. A. Sawano, A. Miyawaki, Directed evolution of green fluorescent protein by a new versatile PCR strategy for site-directed and semi-random mutagenesis. *Nucleic Acids Res.* **28**, E78 (2000).
53. M. Van Bel, F. Silvestri, E. M. Weitz, L. Kreft, A. Botzki, F. Coppens, K. Vandepoele, PLAZA 5.0: Extending the scope and power of comparative and functional genomics in plants. *Nucleic Acids Res.* **50**, D1468–D1474 (2022).
54. J. Westermann, E. Koebeke, R. Lentz, M. Hülskamp, A. Boisson-Dernier, A comprehensive toolkit for quick and easy visualization of marker proteins, protein-protein interactions and cell morphology in *Marchantia polymorpha*. *Front. Plant Sci.* **11**, 569194 (2020).
55. R. Ursache, T. G. Andersen, P. Marhavý, N. Geldner, A protocol for combining fluorescent proteins with histological stains for diverse cell wall components. *Plant J.* **93**, 399–412 (2018).
56. D. Li, E. Flores-Sandoval, U. Ahtesham, A. Coleman, J. M. Clay, J. L. Bowman, C. Chang, Ethylene-independent functions of the ethylene precursor ACC in *Marchantia polymorpha*. *Nat. Plants* **6**, 1335–1344 (2020).
57. G. Sena, X. Wang, H. Y. Liu, H. Hoffhuis, K. D. Birnbaum, Organ regeneration does not require a functional stem cell niche in plants. *Nature* **457**, 1150–1153 (2009).
58. D. Saint-Marcoux, H. Proust, L. Dolan, J. A. Langdale, Identification of reference genes for real-time quantitative PCR experiments in the liverwort *Marchantia polymorpha*. *PLOS ONE* **10**, e0118678 (2015).
59. R. Patro, G. Duggal, M. I. Love, R. A. Irizarry, C. Kingsford, Salmon provides fast and bias-aware quantification of transcript expression. *Nat. Methods* **14**, 417–419 (2017).
60. C. Sonesson, M. I. Love, M. D. Robinson, Differential analyses for RNA-seq: Transcript-level estimates improve gene-level inferences. *F1000Res.* **4**, 1521 (2015).
61. M. I. Love, W. Huber, S. Anders, Moderated estimation of fold change and dispersion for RNA-seq data with DESeq2. *Genome Biol.* **15**, 550 (2014).
62. C. Chen, H. Chen, Y. Zhang, H. R. Thomas, M. H. Frank, Y. He, R. Xia, TBtools: An integrative toolkit developed for interactive analyses of big biological data. *Mol. Plant* **13**, 1194–1202 (2020).
63. J. Xia, D. S. Wishart, Using metaboanalyst 3.0 for comprehensive metabolomics data analysis. *Curr. Protoc. Bioinform.* **55**, 14.10.11–14.10.91 (2016).
64. J. Heyman, H. van den Daele, K. de Wit, V. Boudolf, B. Berckmans, A. Verkest, C. L. A. Kamei, G. de Jaeger, C. Koncz, L. de Veylder, Arabidopsis ULTRAVIOLET-B-INSENSITIVE4 maintains cell division activity by temporal inhibition of the anaphase-promoting complex/cyclosome. *Plant Cell* **23**, 4394–4410 (2011).

**Acknowledgments:** We thank A. Bleys for help in preparing the manuscript. We thank J. Haseloff (University of Cambridge) for sharing OpenPlant toolkit constructs for cloning, A. Goossens (VIB) for sharing AtJAZ constructs for the yeast two-hybrid assay and critical comments, Y. Hirakawa (Gakushuin University) for sharing proMpYUC2\_pENTR/D-TOPO construct, and R. Solano (CNB-CSIC) for sharing Mpcol1-2 mutant materials. **Funding:** This work was supported by Research Foundation-Flanders grant G007218N (B.C. and L.D.V.), Research Foundation-Flanders grant G010820N (Y.L., Y.X., W.V., and L.D.V.), and China Scholarship predoctoral scholarship 201806910058 (Y.L.). **Author contributions:** Conceptualization: Y.L. and L.D.V. Methodology: Y.L., J.H., Y.X., W.V., G.G., and B.C. Investigation: Y.L., J.H., Y.X., W.V., G.G., and B.C. Supervision: L.D.V. Writing—original draft: Y.L. and L.D.V. Writing—review and editing: Y.L., J.H., Y.X., W.V., G.G., B.C., and L.D.V. **Competing interests:** The authors declare that they have no competing interests. **Data and materials availability:** All data needed to evaluate the conclusions in the paper are present in the paper and/or the Supplementary Materials.

Submitted 24 February 2022  
 Accepted 28 June 2022  
 Published 12 August 2022  
 10.1126/sciadv.abo7737